

University of Montana

ScholarWorks at University of Montana

Graduate Student Theses, Dissertations, &
Professional Papers


Graduate School

2022

ARCTIC GREENING: CHARACTERIZING TUNDRA VEGETATION FROM IN-SITU AND REMOTELY SENSED OBSERVATIONS

Shira Ann Ellenson

Follow this and additional works at: <https://scholarworks.umt.edu/etd>

 Part of the [Geographic Information Sciences Commons](#), [Physical and Environmental Geography Commons](#), and the [Remote Sensing Commons](#)

Let us know how access to this document benefits you.

Recommended Citation

Ellenson, Shira Ann, "ARCTIC GREENING: CHARACTERIZING TUNDRA VEGETATION FROM IN-SITU AND REMOTELY SENSED OBSERVATIONS" (2022). *Graduate Student Theses, Dissertations, & Professional Papers*. 12031.

<https://scholarworks.umt.edu/etd/12031>

This Thesis is brought to you for free and open access by the Graduate School at ScholarWorks at University of Montana. It has been accepted for inclusion in Graduate Student Theses, Dissertations, & Professional Papers by an authorized administrator of ScholarWorks at University of Montana. For more information, please contact scholarworks@mso.umt.edu.

ARCTIC GREENING: CHARACTERIZING TUNDRA
VEGETATION FROM IN-SITU AND REMOTELY SENSED
OBSERVATIONS

By

SHIRA ANN ELLENSON

B.S., Cornell University, 2014

Thesis

Presented in partial fulfillment of the requirements for the degree of

Master of Science in Geography, GIS and Cartography Option

The University of Montana

Missoula, MT

Fall Semester 2022

Dr. Anna Klene

Department of Geography

Kevin McManigal

Department of Forest Management

Dr. Carl Seielstad

Department of Forest Management

ACKNOWLEDGMENTS

Sincere gratitude goes out first and foremost to my advisor, Anna Klene, for her endless support, knowledge, and patience in providing guidance and feedback throughout every step of my graduate career. Kevin McManigal for his cartography expertise and reminder that joy and curiosity exist in teaching and learning. To Carl Seielstad for providing a crucial turning point during a roadblock in my analysis. I would like to thank Skip Walker for allowing me to work with his dataset and field instruments. Randy Fulweber at the Toolik GIS office for providing field support and knowledge of photogrammetry software.

I am very grateful for my partner Eli Sturm, my Missoula community, friends, and family for providing an important sounding board throughout this process and encouraging me to maintain a healthy school-life balance

This research was made possible with a grant from the National Science Foundation (OPP-1836377 and OPP-1836381), as well as scholarship support from the Montana Space Grant Consortium (MSGC), Montana Association of Geographic Information Professionals (MAGIP), MontanaView, and DJ&A.

ABSTRACT

Ellenson, Shira, M.S., Fall 2022

Geography

Arctic Greening: Characterizing Tundra Vegetation Change from In-situ and Remotely Sensed Observations

Chairperson: Anna E. Klene

As the Arctic has warmed at twice the rate of the global average, vegetation productivity has also been increasing. While satellite remote sensing is useful for summarizing Arctic-wide trends, changes in tundra species heights, densities, composition, and distribution can be missed at coarse resolution. Smaller, plot-scale studies are necessary to better understand vegetation dynamics at fine scales occurring on the ground.

In 1995, high-resolution traditional aerial photographs and in-situ measurements of vegetation characteristics were taken at a series of plots established on the Alaskan North Slope. Repeat field surveys in 2021 revealed increases in plant cover for deciduous shrubs and graminoids and decreases for bryophytes that were substantial at some sites. The overall mean canopy height doubled from 6.1 to 13.7 cm (individual sites increased 63 to 513%) and overall mean maximum shrub height doubled from 31.7 to 60.0 cm (individual sites increased 26 to 170%) between 1995 and 2021. Tundra vegetation within these plots has changed substantially over this 26-year period.

I used traditional air photos to measure tundra vegetation by applying a modern photogrammetry workflow and LiDAR-based classification to generate canopy height models (CHMs) at varying resolutions. When compared to field measurements, mean point-cloud estimated canopy heights calculated at 10 cm pixel resolution showed differences of 0 to 2.8 cm at sites with mean canopy heights of 2.3 to 5.8 cm. At sites with taller vegetation (mean canopy heights of 13.8 and 18.5 cm) differences were 0.7 and 1.6 cm, respectively, from point-cloud estimates made at 25 cm pixel resolution. Finer resolution CHMs performed better with shorter canopy heights, and coarser resolution CHMs worked better with taller canopy heights. These results suggest that using high-resolution remote sensing paired with in situ measurements can estimate canopy heights for tundra vegetation, allowing small changes to be detected.

This study contributes to the record of fine-scale remote sensing techniques and plot-level vegetation change in the Alaskan Arctic, and supports the need for continued long-term ecological monitoring in a rapidly warming climate.

TABLE OF CONTENTS

1. INTRODUCTION.....	1
1.1 Research Questions	2
1.2 Study Area.....	2
2. MEASURING TUNDRA VEGETATION CHANGE BETWEEN 1995 AND 2021	4
2.1 Background	4
2.1.1 Evidence for Increased Greening and Browning.....	5
2.1.2 Remote Sensing & Arctic NDVI trends	6
2.2 Methods.....	8
2.2.1 Baseline Measurements	8
2.2.2 Recent Measurements.....	9
2.2.3 Data Analysis.....	11
2.3 Results.....	12
2.3.1 Functional Groups	12
2.3.2 Canopy Measurements	16
2.3.3 Maximum Shrub Height.....	18
2.4 Discussion	19
2.5 Conclusion.....	21
3. USING TRADITIONAL AIR PHOTOS TO ESTIMATE TUNDRA VEGETATION HEIGHT	22
3.1 Background	22
3.1.1 Photogrammetry for Vegetation Height	22
3.1.2 Fine-Scale Mapping.....	24
3.2 Methods.....	24
3.2.1 Aerial Surveys	24
3.2.2 Initial Image Processing	26
3.2.4 Point-Cloud Classification, and DSM, DTM, and CHM Production.....	26
3.2.5 Validation Data.....	28
3.3 Results.....	29
3.3.1 Quantitative Assessment of Canopy Heights from the Agisoft Workflow	29

3.3.2 Spatial and Qualitative Assessment of Canopy Heights from the lidR Workflow	30
3.3.3 Quantitative Assessment of Canopy Heights from the lidR Workflow	41
3.3.4 Quantitative Assessment of Maximum Shrub Heights from the lidR Workflow	43
3.4 Discussion	48
3.4.1 Data Acquisition and Processing	48
3.4.2 Interpolation and Pixel Resolution	49
3.5 Conclusion.....	51
DATA AVAILABILITY STATEMENT	53
REFERENCES	54

LIST OF TABLES AND FIGURES

Table 1: Location and Site Description of Flux Study Plots	4
Table 2: Summary of 2021 Field Data.....	10
Table 3: Percent Change in Top of Plant Canopy.....	14
Table 4: Percent Change in Bottom of Plant Canopy	16
Table 5: Canopy Height Summary Table	17
Table 6: Maximum Shrub Height Summary Table.....	19
Table 7: Summary of 1995 Aerial Survey Metadata	25
Table 8: ANOVA Results for Canopy Heights	46
Table 9: ANOVA Results for Maximum Shrub Heights.....	47
Table A1: Functional Groups Percent Cover in 1995 and 2021	52
Figure 1: Study Area.....	3
Figure 2: Flux Plot Layout.....	9
Figure 3: Percent Change in Top of Plant Canopy	13
Figure 4: Percent Change in Bottom of Plant Canopy.....	15
Figure 5: Canopy Heights.	17
Figure 6: Maximum Shrub Heights	18
Figure 7: Agisoft Boxplots.....	30
Figure 8: Flux 1 CHM Maps.....	31
Figure 9: Flux 2 CHM Maps.....	32
Figure 10: Flux 3 CHM Maps.....	33
Figure 11: Flux 4 CHM Maps.....	34
Figure 12: Flux 6 CHM Maps.....	35
Figure 13: Flux 7 CHM Maps.....	36
Figure 14: Flux 8 CHM Maps.....	37
Figure 15: Flux 9 CHM Maps.....	38
Figure 16: Flux 10 CHM Maps.....	39
Figure 17: LidR Box Plots	41
Figure 18: Mean Cloud Estimates vs Mean Canopy Heights	45
Figure 19: Mean Cloud Estimates vs Maximum Canopy Heights	45

1. INTRODUCTION

Shrub expansion has been documented across arctic and alpine tundra ecosystems over the last 70 years. Satellite observations and long-term ecological monitoring show increased vegetation productivity for the same period. However, responses to climate change are not likely to be uniform across a mosaic of land-cover types nor driven by air temperature alone (Elmendorf et al., 2012). Other controls operating at fine scales include glacial history, permafrost characteristics, topography, soil moisture, nutrient availability, and more (Berner et al., 2020). While satellite remote sensing is useful for summarizing Arctic trends, variation in spatial and temporal trends arise due to complex ecosystem interactions which can be missed at coarse resolution (Myers-Smith et al., 2020). Smaller, plot-scale studies are necessary to better understand vegetation changes occurring on the ground.

This project evaluates vegetation change over 26 years on the North Slope of Alaska using field measurements and examines the use of high-resolution aerial photographs to quantify vegetation heights. The results from this study will improve our current understanding of the fine-scale changes (within 1 ha plots) driving complex ecosystem interactions.

In addition to carbon and nutrient cycling, vegetation changes can significantly impact permafrost stability and wildlife habitat, as well as human livelihood and infrastructure. Continued monitoring of vegetation-climate feedbacks is essential to understanding current and future Arctic conditions that have ecological and social implications locally, regionally, and globally (Frost et al., 2019).

1.1 Research Questions

This study seeks to evaluate vegetation change from 1995-2021 at a series of plots on the North Slope of Alaska using field measurements and fine-scale remote sensing techniques. This research will address several main questions:

- *Has the relative height and percent cover of plant functional groups changed within these plots between 1995 and 2021?*
- *Can tundra vegetation heights be measured using traditional air photos from 1995 with modern processing methods? If so, are the estimates accurately capturing mid-canopy heights, maximum shrub heights, or both?*

1.2 Study Area

The research sites used in this study are part of the Circumpolar Active Layer Monitoring (CALM) network. CALM was established in 1991 with the goal of observing the long-term response of active-layer thickness (ALT, soil above permafrost that seasonally thaws) and near-surface permafrost to climate change. CALM monitors these changes over long time-series (multi-decadal) at >240 sites in both hemispheres with participants from 15 countries. In the Kuparuk River Basin of Northern Alaska, a series of 1 ha plots were established by the North Slope Arctic System Science/Land-Atmosphere-Ice Interactions (ARCSS/LAII) Flux Study project in August of 1995 and 1996. The Flux Study was designed to improve understanding of the variables and processes controlling the fluxes of greenhouse gases and future responses to climate variations (Kane & Reeburgh, 1998). Extensive data were collected on vegetation, environmental plot, and soil characteristics. The CALM project has continued annual monitoring of air and soil-

surface temperature at 9 of these sites (Figure 1), and vegetation were resurveyed in 2021 (Table 2). The study area spans the Brooks Range foothills and coastal plain on the North Slope, including CAVM bioclimatic subzones C, D, and E (CAVM, 2003). These sites represent a variety of land-cover types including wet tundra, shrublands, moist acidic tundra, and moist non-acidic tundra. This provides a rare long-term dataset of active-layer thickness and soil temperatures on the North Slope, enabling a time-series analysis. A summary of these sites can be found in **Error! Reference source not found.**

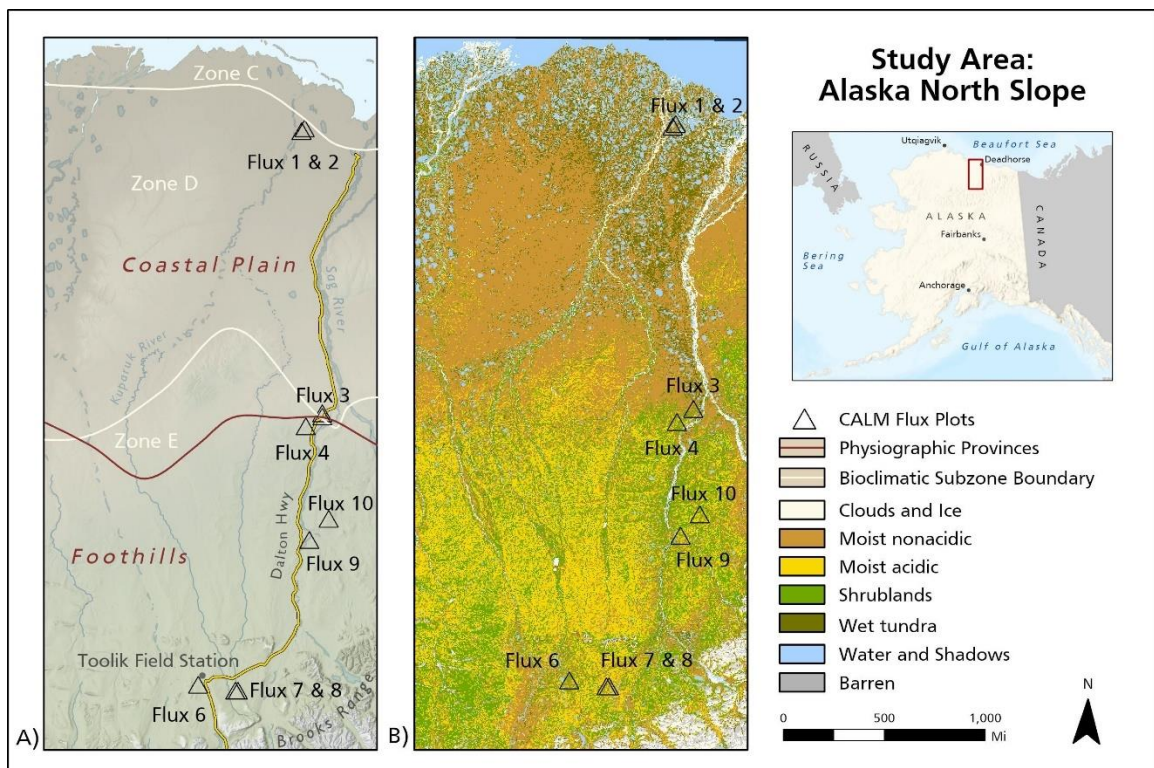


Figure 1: Maps of the study region showing locations of 1 ha Flux Study Plots relative to (A) bioclimatic subzones (CAVM, 2003) and physiographic provinces (Warhafting, 1965), and (B) vegetation type (Auerbach et al., 1996).

Flux Site	Informal Name	Landcover Class/ Physiographic Province	Landform	Latitude (°)	Longitude (°)	Elev. (m)
1	Betty Pingo	Moist Non-acidic/ Coastal Plain	Residual Surface	70.281	-148.944	12
2	Betty Pingo 2	Wet Non-acidic/ Coastal Plain	Low center polygon	70.275	-148.919	12
3	Sagwon MNT	Moist Non-acidic/ Northern Foothills	Hilltop	69.440	-148.670	269
4	Sagwon MAT	Moist Acidic/ Northern Foothills	Hilltop	69.402	-148.799	360
6	Toolik Lake	Water Track/ Southern Foothills	Hillside with small water track	68.623	-149.618	777
7	Lower Imnavait Creek	Wet Acidic/ Southern Foothills	Basin	68.611	-149.314	917
8	Upper Imnavait Creek	Moist Acidic/ Southern Foothills	Hillside	68.610	-149.314	938
9	Sagavanirktok River Island	Riparian Shrubland/ Northern Foothills	Stabilized River Bar	69.0742	-148.7592	349
10	Lupine Hill	Water Track/ Northern Foothills	Hillside with water track	69.129	-148.592	537

Table 1: Table of Flux Study Plot names, land-cover class, physiographic province, location, and elevation (Walker & Bockheim, 1995).

1. MEASURING TUNDRA VEGETATION CHANGE BETWEEN 1995 AND 2021

2.1 Background

Vegetation growth plays an integral role in ecosystem carbon balance as it sequesters atmospheric carbon during photosynthesis and acts as a carbon sink, offsetting climate-sensitive frozen reservoirs in permafrost regions. Permafrost underlies around 24% of the land in the Northern Hemisphere and over 80% of Alaska (Zhang et al., 2003).

Currently, there is about twice as much carbon held in these permafrost regions than is held in the atmosphere (Schurr, 2019). As the climate continues to warm and release stored carbon in an accelerated feedback, the Arctic may shift and become a carbon source (Schurr, 2019). Vegetation-climate feedbacks associated with Arctic greening

have global implications, yet there is considerable uncertainty in the projected rates and degrees of change (IPCC, 2014).

Tundra vegetation change has been identified as one of the clearest examples of the terrestrial impacts of climate change (IPCC, 2014). As the Arctic warms at twice the rate of the global average, vegetation is responding with changes in species composition, density, and distribution. Observed changes in vegetation have been termed Arctic “greening” and “browning” (NASEM, 2019). Arctic greening refers to an increase in vegetation growth and productivity, while browning is a decrease in vegetation, often indicating reduced health, disturbance, or the expansion of water bodies (Myers-Smith et al., 2020; NASEM 2019). Changes in tundra vegetation produce a series of cascading effects in the structure and function of Arctic ecosystems, including climate feedbacks, and changes in permafrost (perennially frozen ground), snow cover, wildlife habitat, and human communities (Epstein et al., 2012). Interactions between vegetation, nutrient cycling, permafrost, surface reflectance, ground temperatures, and disturbance can all contribute to positive and negative feedback mechanisms that have implications regionally and beyond (Myers-Smith et al., 2011).

2.1.1 Evidence for Increased Greening and Browning

Some of the first evidence of field-based greening in the Alaskan Arctic used repeat photography to show distinct and dramatic increases in the height and diameter of individual shrubs including *Betula Nana*, *Alnus Crispa*, and *Salix Sp.* (Sturm et al., 2001; Tape et al., 2006). The most discernable changes were in hillslopes and valley bottoms. There have been other long-term field studies that have confirmed similar results across

the Arctic and found biome-wide increases in vascular plant abundance and height (Bjorkman et al., 2018; Elmendorf et al., 2012; Frost & Epstein 2013; Myers-Smith et al., 2011). In particular, shrub observations have been characterized by: 1) infilling of existing patches, 2) increase in growth, and 3) advancing shrubline (Myers-Smith et al., 2011). Increases in size-related traits have been identified as adult plant height and leaf area (Bjorkman et al., 2018). These studies indicate a strong association between the degree of summer warming and increase in vascular plant abundance (Elmendorf et al., 2012; Tape et al., 2006). They also highlight soil and surface moisture as key influences on the strength and direction of vegetation growth (Bjorkman et al., 2018), emphasizing that environmental factors are vital to biotic community productivity.

In-situ Arctic studies have also observed browning events, largely attributed to disturbance events such as fire, permafrost degradation, erosion, increased surface wetness, and local disease outbreaks (Myers-Smith et al., 2020). However, the magnitude, spatial variation, and drivers of Arctic greening and browning are not well understood (Myers-Smith et al., 2020).

In this study, we contribute to the long-term record of in-situ measurements in Northern Alaska by resampling vegetation that was last surveyed in 1995 at a series of plots at which air and soil-surface temperatures been monitored continuously. Long-term vegetation records are needed to quantify landscape change in response to accelerated rates of tundra warming.

2.1.2 Remote Sensing & Arctic NDVI trends

Evaluating current and future Arctic conditions requires an extensive spatial perspective that aggregates numerous landscape elements (Epstein et al., 2012; Frost et al., 2019). Remotely-sensed datasets allow the quantification of past spatial and temporal change across complex and remote landscapes like the Arctic. The normalized difference vegetation index (NDVI), an index of the greenness of vegetation, is a common tool used in remote sensing to assess plant productivity and strongly correlates with tundra vegetation biomass (Raynolds et al., 2011; Tucker, 1979). NDVI quantifies differences in vegetation by measuring the reflection of infrared and red wavelengths of light where:

$$\text{NDVI} = (\text{NIR} - \text{R}) / (\text{NIR} + \text{R}).$$

The longest temporal datasets of NDVI have been produced from satellite-based sensors with broad spatial coverages and varying sampling frequencies (Myers-Smith et al., 2020). The most commonly used are derived from the Advanced Very High Resolution Radiometer sensor (AVHRR; 1982 to present, global coverage twice daily) on NOAA satellites, the Moderate-resolution Imaging Spectroradiometer sensor (MODIS; 2000 to present, 16 day intervals) on NASA satellites, and from the Landsat sensors (1972 to present, 16 day intervals; Myers-Smith et al., 2020). The GIMMS-3g record, an AVHRR-derived dataset at 8 km resolution, shows that roughly 33% of the Pan-Arctic has substantially greened with the strongest increase seen in Alaska's North Slope (Pinzon and Tucker 2014). This coincides with amplified warming trends seen for the same temporal period (IPCC, 2014). MODIS NDVI records (1 km resolution) from 2000 to 2015 show similar increases in greening for the North Slope (Rochsa & Wright, 2019). There are several studies from long-term field monitoring (Elmendorf et al., 2012; Myers-Smith et al., 2019) and historical imagery (Sturm et al., 2001; Tape et al., 2006),

that show similar greening trends. Conversely, coarse scale (>1 km) greening trends do not always correspond with observations on the ground or with finer-scale remote sensing data. Landsat records (30 m resolution) and local field reports showing considerable heterogeneity on the North Slope at finer scales (Pattison et al., 2015; Raynolds et al., 2013), little change in ground vegetation at some locations (Jorgenson et al., 2015), and warming-induced browning events (Bhatt et al., 2013; Raynolds & Walker 2016).

Heterogeneity in vegetation response to climate warming has been linked to complex ecosystem interactions and site factors such as changes in nutrient availability (Chapin et al., 1995), ecological disturbance (Jorgensen et al., 2015), permafrost degradation (Jin et al., 2021), soil moisture (Bjorkman et al., 2018), and increased surface wetness (Raynolds & Walker 2016). More field-based studies and finer resolution remote sensing data are needed to elucidate complex ecosystem interactions occurring on the ground.

2.2 Methods

2.2.1 Baseline Measurements

Field sampling methods were based upon protocols used in the 1995 North Slope ARCCS/LAII Flux Study Plots (Walker & Breen, 2017). Field samples were taken at a series of sites along a north-south gradient representing four homogenous land-cover types (moist nonacidic tundra, moist acidic tundra, wet tundra, and shrublands) and some heterogenous plots. Each site consists of a 100 × 100 m plot with corners and center point marked in the field (Figure 2). Six transects¹ were

¹ Some descriptions of these plots refer to these as 3 transects, defining them as 100 and 140 m, respectively, which intersect at the center.

measured from the center point out to the edge of the plot and marked with wire flags spaced at 5 m intervals. Walker and Gallant labeled these as “left” or “right” of the diagonal, as well as “positive” or “negative” of the center.

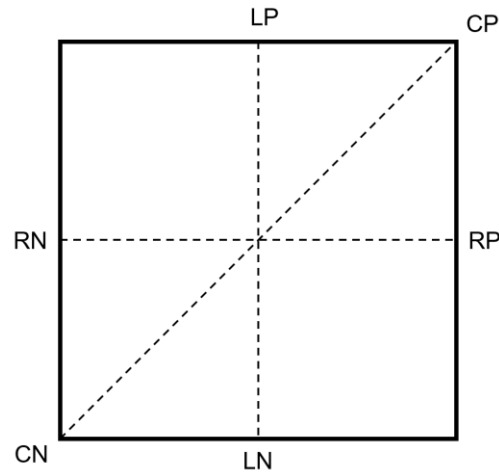


Figure 2: Diagram of the layout of a 100×100 m Flux plot, with 6 transects (4×50 m, “RP”, “RN”, “LP”, “LN” and 2×70 m transects, “CP”, “CN”) radiating from the center

Species composition and canopy height was recorded at each meter along the 6 transects, for a total of ~340 points. The center point was not sampled. Species occurrence at the top and bottom of the plant canopy was sampled using a Buckner optical point sampling device (Buckner, 1985). Canopy height was measured from the top of the moss layer to the height of a point intersected in the plant canopy. A list of vegetation communities was also made for each site. The location of vegetation communities, maximum shrub heights within the communities, and transitions between communities were recorded along each transect (Walker & Bockheim, 1995).

2.2.2 Recent Measurements

Species composition, canopy height, and maximum shrub heights were repeated by

replicating methods used in 1995. A summary of 2021 field data is in Table 2.

Site	Name	Species Comp.	Canopy Height (Every 5 m)	Max Shrub Height*	Max Shrub Height (Every 5 m)	Oblique Photos
Flux 1	Betty Pingo	No	No	NA	NA	No
Flux 2	Betty Pingo 2	No	No	NA	NA	No
Flux 3	Sagwon 3	CP, CN	CP, CN	All	No	CP, CN
Flux 4	Sagwon 4	CP, CN	CP, CN	NA	CP, CN	CP, CN
Flux 6	Toolik	CP, CN	CP, CN	All	CP, CN, RP, RN	CP, CN
Flux 7	Lower Imnaviat Creek	CP, CN	CP, CN	All	No	CP, CN
Flux 8	Upper Imnaviat Creek	CP, CN	CP, CN	All	No	CP, CN
Flux 9	Sag. River Island	No	No	No	CP, CN, LP, LN	No
Flux 10	Water Track	CP, CN	CP, CN	All	No	CP, CN

No = did not collect, will in 2022

NA = No record from 1995

All = all transects

* = Within vegetation communities defined by Walker and Gallant (1995)

Table 2: Table summarizing the field data collected at each Flux Plot in summer 2021, including species composition, canopy height, maximum shrub heights and oblique photographs.

Flux 1 and 2 were not surveyed due to COVID-19 challenges. Flux 5 was primarily barren ground, was not monitored as thoroughly after summer 1997, and was not included in these analyses.

In spring 1996, Flux 9 was flooded by the Sagavanirktok River and the stakes, flags, and other equipment were washed away; it was not revisited until 2021. The center of the site was found to within ~5 m and the transects were relocated using a compass. Flagging tape was tied to tall shrub branches to aid future relocation.

Species composition and canopy height measurements were collected every 5 m along select transects instead of each meter due to time constraints. Maximum shrub

heights were recorded along each transect within the vegetation communities defined in 1995 (Walker & Bockheim, 1995). Flux Plot 4 did not have a vegetation community record for maximum shrub height taken in 1995. Maximum shrub height within vegetation communities was not sampled at Flux Plot 9 due to relocation challenges. For these reasons, a supplementary maximum shrub height was measured in 2021 within each 5 m interval along select transects at Flux Plots 4, 6, and 9. Flux 6 had been sampled in 1995, but resampling it in 2021 allowed comparison of the method used by Walker in 1995, and that taken within every 5 m in 2021. For documentation, oblique photos of the vegetation were taken every 5 m along the center transects.

2.2.3 Data Analysis

Plant species data from 1995 and 2021 were aggregated into six common Arctic functional groups (growth forms): bryophytes, deciduous shrubs, evergreen shrubs, forbs, graminoids, lichen, and litter. Functional group observations were taken in both the top and bottom of the plant canopy and compared to 1995 measurements every 5 m on the diagonal (CP and CN) transects, resulting in ~30 points per plot. Vegetation canopy heights were collected every 5 m on CP and CN transects, for a total of 28 points per plot. They were compared to the 1995 measurements every 5 meters across center transects (a subset of those taken every 1 m).

Both maximum shrub height measurements (within vegetation communities and every 5 m) were summarized by plot and compared to 1995 vegetation community data across all transects. Statistics at Flux 6 were computed to allow comparison between maximum shrub heights measured within communities and those measured every 5 m.

2.3 Results

2.3.1 Functional Groups

Functional groups were assessed at the top and the bottom of the plant canopy. The following results compare 2021 measurements to 1995 measurement every 5 m on the center transects only². Change was detected between 1995 and 2021 at the top of the plant canopy for four of the seven plant growth forms (Figure 3 and Table 3). Due to the low sample size, changes of 7.1% indicates change in just two observations along the center transects. Graminoids increased (3 to 38%) at all sites. Bryophyte cover decreased (7 to 39%) at all sites. Decreases (3 to 15%) in litter were found at 5 of the 6 sites. Deciduous shrubs increased (4 to 18%) at Flux 3, 6, 7, 8, and decreased (5%) slightly at Flux 10. Evergreen shrubs decreased by 20% at Flux 6, but showed little change at other sites. No notable changes (< +/-3%) were observed for lichen. Forbs increased (7%) at Flux 3, 4, and 10, and decreased (11%) at Flux 8. Percent cover for the plots in 1995 and 2021 are shown in Table A1 of the Appendix.

² Initial comparisons were made between 2021 measurements (every 5 m on center transects) and 1995 measurements every 5 m on all transects. Differences in percent change of functional groups were less 10% from those presented here, and trends remained the same.

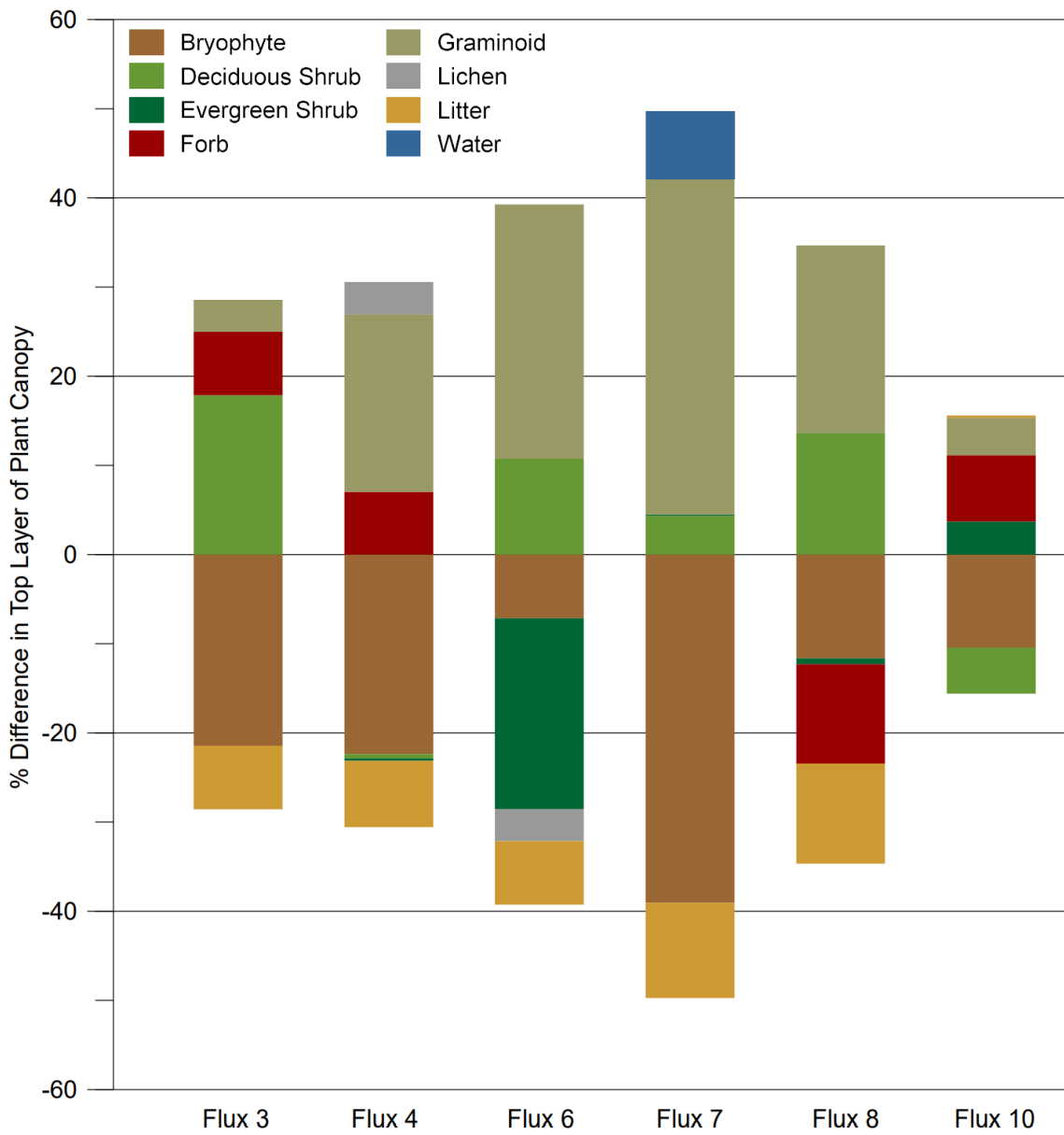


Figure 3: Stacked bar chart showing difference in percent cover (by functional group) in the top of plant canopy between 1995 and 2021 at each Flux Plot.

Functional Group	Flux 3 (%)	Flux 4 (%)	Flux 6 (%)	Flux 7 (%)	Flux 8 (%)	Flux 10 (%)
Bryophyte	-21	-22	-7	-39	-12	-10
Deciduous Shrub	18	-1	11	4	14	-5
Evergreen Shrub	0	0	-21	0	-1	4
Forb	7	7	0	0	-11	7
Graminoid	4	20	29	38	21	4
Lichen	0	4	-4	0	0	0
Litter	-7	-7	-7	-11	-11	0
Water	0	0	0	8	0	0

Table 3: Summary table showing difference in percent cover (by functional group) in top of plant canopy between 1995 and 2021 at each Flux Plot. Comparison was made every 5m on center transects only.

Similar trends were found for the bottom of the plant canopy (Figure). Graminoids increased (7 to 37%) at all sites except Flux 4 where no change (< 1%) was found. Bryophytes decreased (16 to 42%) substantially across all sites except at Flux 6 where it increased (11%). Litter decreased (3 to 15%) at all sites except Flux 3 (+7%). Deciduous shrubs increased (3 to 15%) at Flux 3, 4, 8, 10, decreased (10%) at Flux 7, and showed no change (0%) at Flux 6. Evergreen shrubs increased (25%) at Flux 4, decreased (21%) at Flux 6, but showed little change (+/-4%) at the remaining sites. Little change was observed for lichen or forbs.

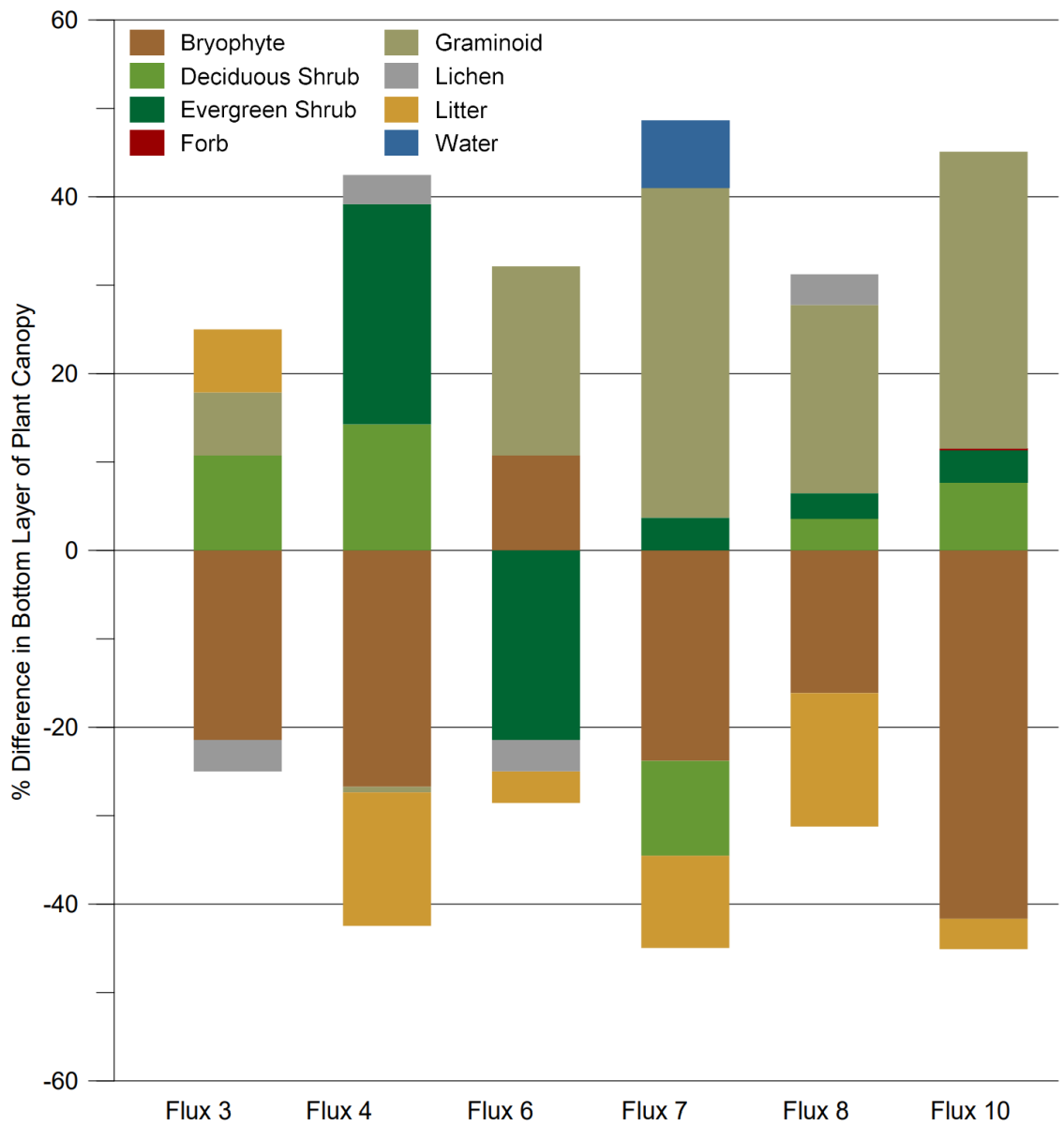


Figure 4: Stacked bar chart showing difference in percent cover (by functional group) in the bottom of plant canopy between 1995 and 2021 at each Flux Plot.

Functional Group	Flux 3 (%)	Flux 4 (%)	Flux 6 (%)	Flux 7 (%)	Flux 8 (%)	Flux 10 (%)
Bryophyte	-21	-27	11	-24	-16	-42
Deciduous						
Shrub	11	14	0	-11	4	8
Evergreen						
Shrub	0	25	-21	4	3	4
Forb	0	0	0	0	0	0
Graminoid	7	-1	21	37	21	34
Lichen	-4	3	-4	0	3	0
Litter	7	-15	-4	-10	-15	-3
Water	0	0	0	8	0	0

Table 4: Summary table showing difference in percent cover (by functional group) in top of plant canopy between 1995 and 2021 at each Flux Plot.

2.3.2 Canopy Measurements

Plant canopy heights showed substantial growth across all sites (Figure 5 and Table 5), with the overall average height doubling from 6.1 cm to 13.7 cm between 1995 and 2021. Most notably, Flux 3 mean canopy height increased by 293% and Flux 7 increased by 513%.

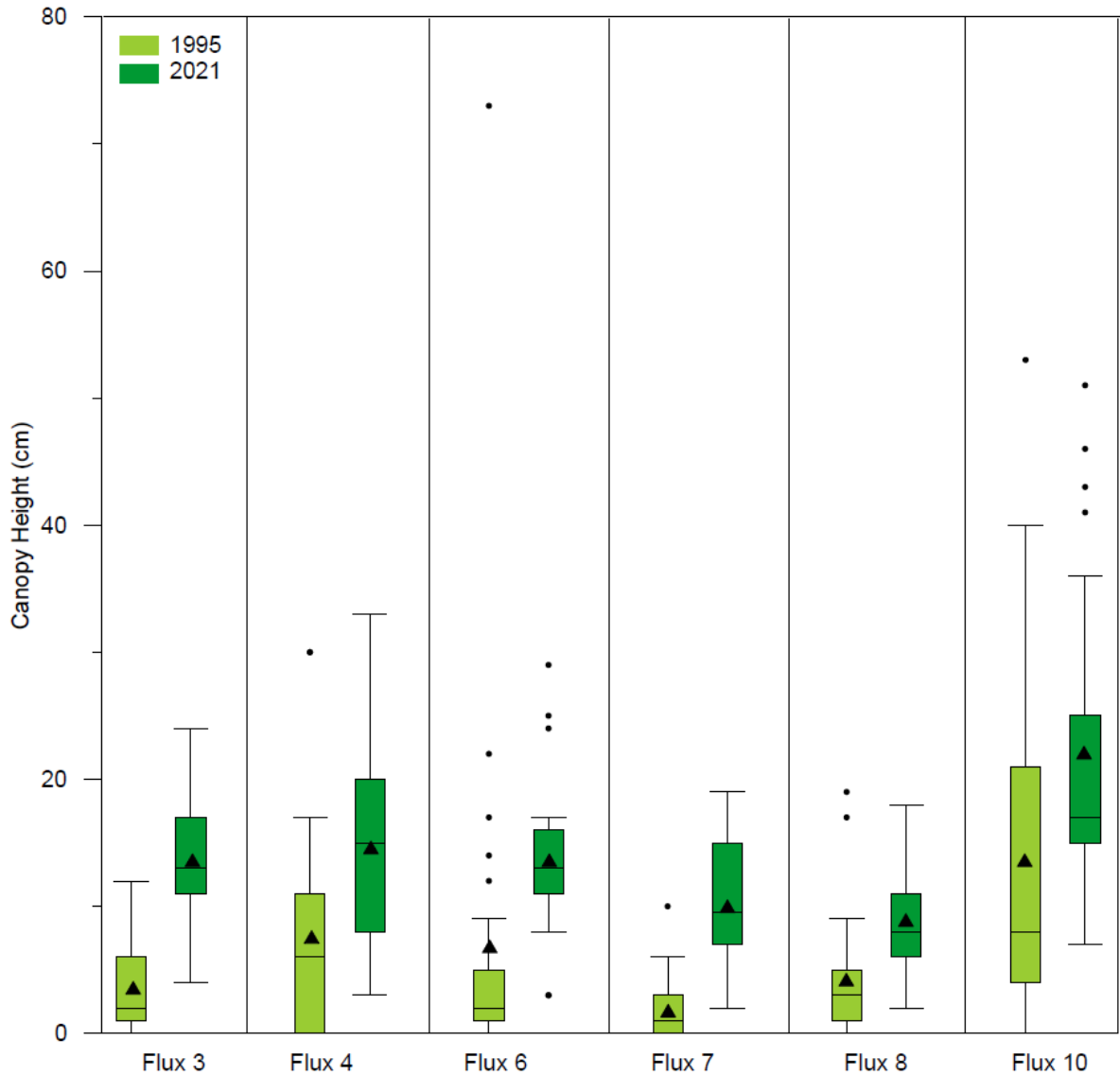


Figure 5: Boxplots showing quartiles and medians comparing canopy heights measured every 5 m along the center transects in 1995 and 2021. Mean values marked by triangles. Sample size at each plot in 1995 and 2021 was 28.

Plot	1995 Mean	2021 Mean	Percent Change (%)
Flux 3	3.4	13.5	293
Flux 4	7.4	14.5	95
Flux 6	6.7	13.5	101
Flux 7	1.6	9.9	513
Flux 8	4.1	8.8	115
Flux 10	13.5	21.9	63

Table 5: Mean canopy heights and percent change in 1995 and 2021.

2.3.3 Maximum Shrub Height

Maximum shrub heights increased across all sites, with considerable increases found at plots with more shrubs and more moisture (Figure 6 and Table 6). Flux 6 increased by 78%, Flux 7 increased by 170%. Flux 9 mean shrub height increased by 127%, and Flux 10 increased by 75%. The most common shrubs observed were *Salix spp.* and *Betula nana*. Across all sites, mean maximum shrub height doubled from 31.7 cm to 60.0 cm with data between 1995 and 2021.

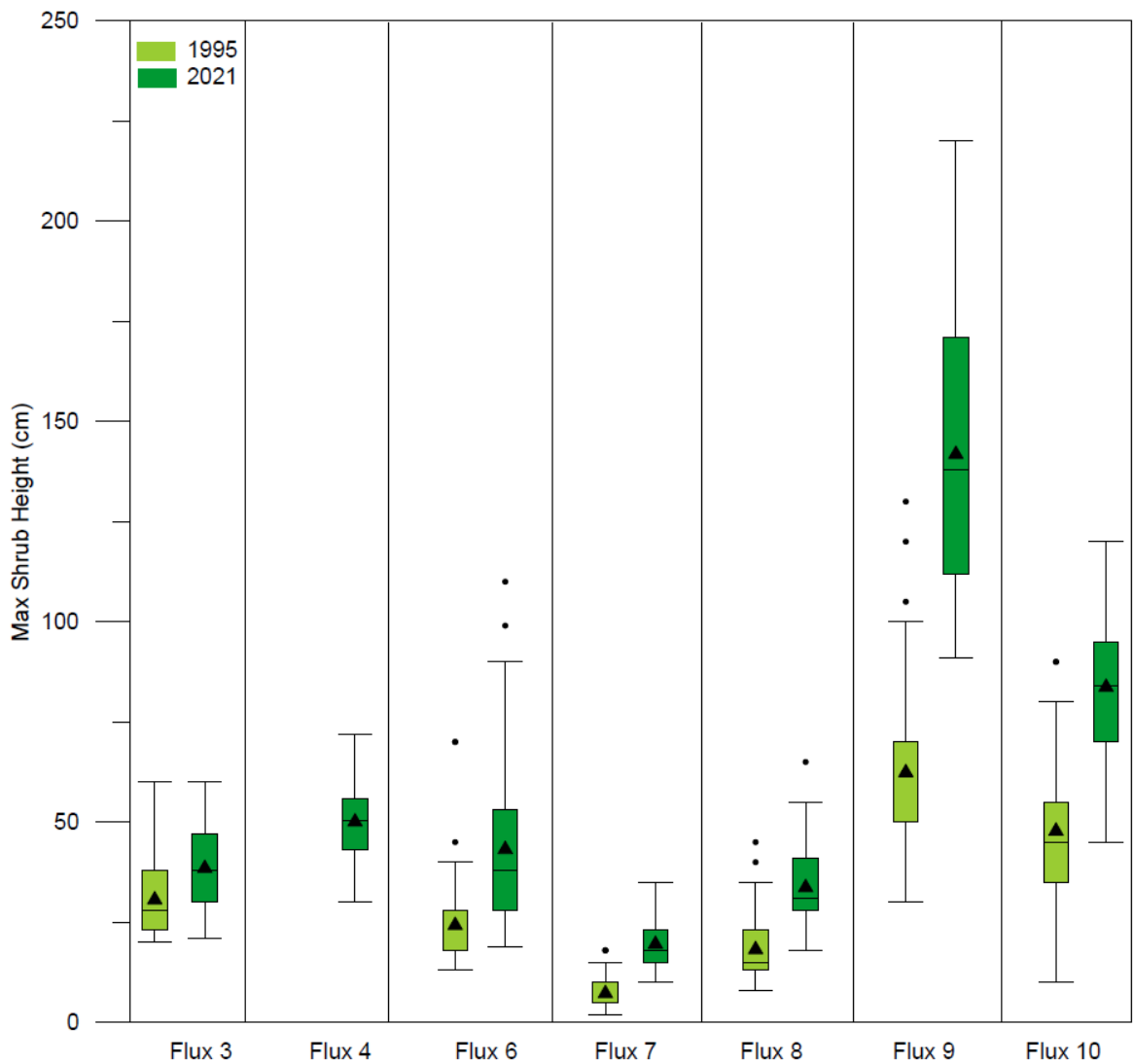


Figure 6: Boxplots showing quartiles and medians comparing maximum shrub heights measured within vegetation communities defined in 1995 and resampled in 2021 at each Flux Plot. Mean values marked by triangles.

Plot	1995 Mean (cm)	2021 Mean (cm)	Change (%)	N in 1995	N in 2021
Flux 3	30.6	38.5	26	25	24
Flux 4	NA	50.1	NA	NA	28
Flux 6	24.2	43.1	78	51	119
Flux 7	7.2	19.6	170	87	84
Flux 8	18.2	33.7	85	32	32
Flux 9	62.4	141.8	127	36	54
Flux 10	47.8	83.7	75	50	50

Table 6: Mean maximum shrub heights, percentage change, and sample sizes in 1995 and 2021.

2.4 Discussion

This study provides plot-level evidence for changes in vegetation over a 26-year period on the North Slope of Alaska. In the top and bottom of the plant canopy, we found increases in graminoids and deciduous shrubs, and decreases in bryophytes and litter. We also found substantial increases in canopy height and maximum shrub height.

In-situ increases in deciduous shrub cover and graminoids is well-documented throughout the Arctic (Elmendorf et al., 2012; Myers Smith et al., 2011; Tremblay et al., 2012) and the North Slope (Sturm et al., 2001; Tape et al., 2006). Tundra plant community composition is shifting towards more shrub and graminoid dominated cover (Myers-Smith et al., 2019). Decreases for bryophyte abundance corresponds with other plot-level studies in the Arctic (Elmendorf et al., 2012; Jorgensen et al., 2015). Bryophyte reduction has been largely attributed to shading from increased shrub cover (Chapin et al., 2003); as shrubs expand in growth and vigor, they outcompete other growth forms.

Increased height and cover of deciduous shrubs and graminoids and decreased bryophyte cover have been found in warming experiments (Elmendorf et al., 2012; Walker et al., 2006), suggesting that changes in vegetation productivity is a direct response to climate

warming. While the main driver for increased vascular plant abundance is linked to increases in local summer warming temperatures (Berner et al., 2020; Elmendorf et al., 2012), recent work supports increased growing season length and deepening active-layer depths as also contributing (Myers-Smith et al., 2019).

Results from this study are consistent with other long-term monitoring records of increased mean canopy height and maximum shrub height (Elmendorf et al., 2012, Myers Smith et al., 2011). Driven by favorable growing conditions and increases in functional group abundance, in-situ observations show that tundra vegetation is becoming taller (Myers Smith et al., 2019). Changing vegetation, particularly increasing height (Bjorkman et al., 2018), has important feedbacks to tundra ecosystem function and carbon cycling. Complex ecosystem processes associated with modifications in vegetation structure may either mitigate or exacerbate warming in tundra ecosystems (Wookey et al., 2009).

Decreased litter may have been due to differences in phenology between July 1995 and 2021. While more litter would be expected later in the season, slight differences in sampling methods and sample size may have also led to this finding.

The findings from this study align with satellite-derived patterns of Arctic greening on the North Slope (Frost et al., 2021; Guay et al., 2014), where tundra greenness is positively correlated with graminoid, shrub, and ecosystem productivity at field sites (Berner et al., 2020). Arctic greening can alter important ecosystem processes including nutrient cycling, permafrost depth, and biodiversity, and have significant impacts on global carbon feedbacks (Frost et al., 2019).

2.5 Conclusion

These repeat field surveys in 1995 and 2021 on Alaska's North Slope show similar results from other studies in northern Alaska, and across the tundra biome as a whole. Percent cover increased for deciduous shrubs and graminoids, and decreased for bryophytes. Across all sites, overall mean canopy height and overall mean maximum shrub height doubled on average between 1995 and 2021. Most plots showed substantial change over the study period. This study contributes to the record of plot-level vegetation change in the Alaskan Arctic, and supports the value of continued long-term ecological monitoring in a rapidly warming climate.

3. USING TRADITIONAL AIR PHOTOS TO ESTIMATE TUNDRA VEGETATION HEIGHT

3.1 Background

3.1.1 Photogrammetry for Vegetation Height

Traditional aerial photography is one of the oldest forms of remotely sensed data and provides users with a valuable archive of past landscapes (Morgan et al., 2010). Aerial photographs provide the longest-available, temporally continuous, and spatially complete historic record, offering opportunity for fine-scale change analysis pre-dating digital satellite imagery (Morgan et al., 2010). Several studies have used traditional aerial photos to document long-term vegetation change in the Arctic (Tape et al., 2006; Myers-Smith et al., 2011), yet few have utilized stereoscopic information and therefore could not report findings on vertical change. The implicit depth information contained in overlapping, offset images allows for three-dimensional reconstruction of objects through photogrammetry analysis.

Photogrammetry is commonly used to make precise spatial measurements of three-dimensional objects and terrain features from two-dimensional images and is valuable for studying fine-scale landscape change (Alonzo et al., 2020). The same concepts and basic geometric principles apply to both traditional hardcopy (analog/film) and modern (softcopy or digital) photogrammetry (Lillesand et al., 2008). When two photos are taken from slightly different viewing angles, ‘lines of sight’ can be estimated from each camera location to points on an object (Carrivick et al., 2016). The intersection of these lines is measured by triangulation and used to reconstruct the three-dimensional location. By repeating this for many locations, a point cloud can be generated (Carrivick et al., 2016).

When digitally scanned, traditional aerial photographs can utilize modern softcopy techniques including image-based terrain extraction algorithms and automatic feature detection.

Photogrammetry-derived point clouds from traditional aerial photos or Unmanned Aerial Vehicles (UAVs) result in a density up to 10× greater than other techniques including airborne and terrestrial LiDAR scanners (Cunliffe et al., 2016, Fraser et al., 2016), which can influence DTM accuracy and ground-point classification (Zhang et al., 2022). Color-infrared aerial photos may be used to estimate vegetation biomass (NDVI) through spectral reflectance measurements alone (Poley and McDermid, 2020), and combined with the utility of structural information from point clouds, vegetation height measurements may be derived on a sub-meter scale simultaneously (Cunliffe et al., 2020; Fraser et al., 2016).

Measuring vegetation heights from aerial photogrammetry using UAVs has been done in the Canadian tundra (Cunliffe et al., 2020, Fraser et al., 2016), southcentral Alaska (Alonzo et al., 2020), and grassland ecosystems (Cunliffe et al., 2016). Several studies have paired photogrammetry with LiDAR scanning, yielding meaningful biomass estimates at fine spatial scales (Greaves et al., 2015, 2019).

Point-cloud based analyses of aerial photos could potentially provide height information on past vegetation in Arctic landscapes to complement existing analysis of vegetation extent. However, estimating canopy heights using point clouds derived from traditional aerial photographs has yet to be tested in a tundra environment where vegetation is highly varied and dwarfed. This study explores using relatively high-resolution aerial photos (1:3000) to quantify vegetation heights.

3.1.2 Fine-Scale Mapping

Remote sensing is useful for monitoring Arctic changes at a variety of spatial and temporal scales; however, there is some disagreement between satellite-based and in-situ measurements that may reflect sub-pixel differences (Myers-Smith et al., 2020). Tundra vegetation communities are low-statured (<2 m) and extremely spatially heterogeneous at fine scales (<1 m²; Greaves et al., 2019). Mapping large areas of low-stature vegetation at coarse resolution using satellite remote sensing such as the AVHRR and MODIS inadequately captures the variability of Arctic landscapes. Fine-scale remote sensing techniques are needed to more accurately characterize the spatial heterogeneity and diversity of tundra vegetation. The objective of this study was to test the utility of point clouds derived from traditional aerial photos to measure tundra canopy heights from 1995 at multiple sites on the North Slope.

Fine-scale remote sensing measurements of tundra ecosystems represent an important scale gap between biome-wide, satellite-based remote sensing and in situ observations (Cunliffe et al., 2020). This is the first study to focus on pairing modern photogrammetry methods with traditional aerial photos and in-situ measurements, and may offer baseline measurements to aid in quantification of long-term vegetation change in the Alaskan Arctic.

3.2 Methods

3.2.1 Aerial Surveys

Several stereo color-infrared (CIR) aerial photographs of each Flux Study plot were obtained by Aeromap Inc. during two missions in July and August 1995. All photos were taken from a mounted film camera at a flying height of 1,500 ft and resolution of 1:3000.

The original film was re-scanned at 12 microns (~2,136 DPI) by Quantum Spatial, resulting in a ~7 cm pixel. Aerial survey metadata are shown in Table 7. The corners and center coordinates of the plot were surveyed at each Flux Plot in 1995 and used as ground control points (GCPs) to georeference the images for Flux Plots 6, 7, and 8 in the originally collected coordinate system, NAD27 UTM Zone 6N. GCPs for Flux 1, 2, 3, 4, 9, and 10 were obtained by rubber-sheeting the corners and centers of the plot on the raw images to base imagery obtained from the Alaska Division of Geological and Geophysical Surveys (DGGs) using the modern coordinate system, NAD83 UTM Zone 6N. All Z values were extracted from the Arctic DEM under the assumption that these points remained vertically stable from 1995 to 2021. Although seasonal heave and subsidence is known to occur within the study area, no vertical data were available in 1995 (Little et al. 2003; Shiklomanov et al. 2013). Camera orientation parameters and fiducial mark coordinates were used from the camera calibration report provided by Quantum Spatial. While initial coordinate information was incorrect, the Agisoft Metashape Support Team assisted in correcting them.

Plot	Date	Time	Camera System	Lens
Flux 1	7 July 1995	NA	Jena LMK 1000	Jena Lamegon PI/C
Flux 2	7 July 1995	NA	Jena LMK 1000	Jena Lamegon PI/C
Flux 3	7 July 1995	NA	Jena LMK 1000	Jena Lamegon PI/C
Flux 4	9 August 1995	NA	Jena LMK 1000	Jena Lamegon PI/C
Flux 6	18 July 95	NA	Zeiss RMK Top 15	Zeiss Pleogon A3/4
Flux 7	7 July 1995	2:20 PM	Jena LMK 1000	Jena Lamegon PI/C
Flux 8	7 July 1995	2:20 PM	Jena LMK 1000	Jena Lamegon PI/C
Flux 9	7 July 1995	NA	Jena LMK 1000	Jena Lamegon PI/C
Flux 10	7 July 1995	1:20 PM	Jena LMK 1000	Jena Lamegon PI/C

Table 7: A summary of 1995 aerial survey metadata for each set of photographs flown, including date, time, camera, system and camera lens. NA indicates the time was not recorded. All photos were taken at a flying height of 1,500 ft and focal length of 153 mm.

3.2.2 Initial Image Processing

Agisoft Metashape was utilized for photogrammetry analysis and point-cloud generation. Image processing followed a standard photogrammetric workflow to produce 3D spatial data as suggested by Agisoft Metashape (Agisoft User Manual, 2022). All photos were successfully aligned to create a sparse cloud using “High Accuracy” and “Generic Preselection” parameters (camera coordinates were unknown). “Gradual Selection” of points was utilized to remove points representing a high amount of noise or with a high reprojection error within the sparse cloud. The criteria selected for removal of approximately 10% of error-producing points were “Reconstruction Uncertainty” (the accuracy of point triangulation within the cloud) and “Projection Accuracy” (points within the projection that were poorly localized). The sparse cloud was then optimized to readjust the estimated point coordinates and camera parameters while minimizing error. High-density point clouds (~200 points/m²) with mild depth filtering (optimal for areas with meaningful small details) were successfully created of each 1-hectare plot and surroundings.

3.2.4 Point-Cloud Classification, and DSM, DTM, and CHM Production

Following examination of the DSM using standard Agisoft procedures (“Classify Ground Points”, “max angle: 15°”, “max distance: 0.05 m” and “cell size: 0.1 m”), DTM (built from the Classified Points with automatic filtering), and CHM (built from the remaining unclassified points with automatic filtering) products, alternate methods of point-cloud classification and image analysis were utilized.

To reduce computational processing time, the georeferenced, unclassified dense point clouds (processed as described in sections 3.2.1 Aerial Surveys and 3.2.2 Initial Image Processing) were clipped to each Flux Plot extent then exported. After importing into R

using the *lidR* package the following steps were used to perform dense-cloud classification and DSM, DTM, and CHM generation:

1) Outliers (noise) were classified and removed by using a Statistical Outliers Removal (SOR) filter. For each point, the mean distance was calculated to its k-nearest neighbors. Points that were farther than the mean plus a multiplier of the standard deviation were removed (Rousell & Auty, 2022). K was set to 10 and the multiplier to 3.

2) Ground points were classified using a Cloth Simulation Filter (CSF) algorithm developed by Zhang et al., (2016). The point cloud was inverted, and a simulated cloth with a given mass was used to “cover” the inverted surface. The interactions between the cloth nodes and the corresponding points are examined to determine cloth-node locations and approximate the ground surface. Parameters were selected by testing a range of values at the sites with the tallest and shortest vegetation, then selecting those which optimized the classification: slope smooth: False, class threshold: 0.1 m, cloth resolution: 0.072 m, cloth rigidity: 3, iterations: 500, and time step: 0.65.

3) A function was created to find the minimum point over a user-defined grid, resulting in a rasterized ground layer (DTM) of only the classified ground points. A 3×3 moving window was then applied to smooth the raster and remove missing values.

4) A DSM was created by implementing a points-to-raster method. For each pixel of the output raster the function “attributed the height of the highest point found” (Rousell & Auty, 2022). In this algorithm, a user-defined radius of a sub-circle was chosen in which each point was replaced by 8 additional points. This simulated that each point was more representative of a disc, densifying the point cloud and smoothing the resulting CHM so

that it returned fewer empty pixels. The sub-circle radius was set to 10 cm. Kriging was then used to spatially interpolate between any remaining missing pixel values.

5) The CHM was calculated by subtracting the DTM from the DSM.

6) Six transects with point spacings of 1 m were digitized for each Flux Plot and CHM values were extracted of the ~340 canopy height estimates for each plot. These were averaged for each CHM at each Flux Plot and compared to the mean in-situ measurements from 1995.

This process was repeated at systematically varied resolutions for a series of DSM and DTM (and resulting CHM) combinations. The spatial resolution utilized affects the number of points within each pixel of a DSM or DTM generated from a point cloud; a finer resolution will have less points in each cell than at a coarser resolution. More points within a grid cell can lead to information loss, and finer grid cell resolutions may contain more interpolated pixel values (Vepakomma et al., 2008). For these reasons, varying resolution were used to generate CHM surfaces. Resolution combinations for CHM products were: 0.1 m (DSM) / 0.1 m (DTM), 0.25 m (DSM) / 0.25 m (DTM), 0.5 m (DSM) / 0.5 (DTM), 1.0 m (DSM) / 1.0 m (DTM), 2.0 m (DSM) / 2.0 m, 0.1 m (DSM) / 0.25 m (DTM), 0.25 (DSM) / 0.5 (DTM), 0.25 m (DSM) / 1.0 (DTM), and 0.5 (DSM), / 1.0 m (DTM). For combinations with unequal resolution, DTMs were re-sampled to match finer resolution DSMs before the CHM was calculated. All modeled measurements were summarized by plot and compared to 1995 field observations.

3.2.5 Validation Data

Field measurements from the North Slope ARCCS/LAII Flux Study Plots were used to validate cloud-based estimates (Walker & Breen, 2017). Each site consisted of a 100 m ×

100 m plot with 6 transects radiating from the center point (Figure 2). Canopy heights were recorded at every meter along each transect, for a total of 340 observations. Canopy height measurements were recorded from the top of the moss layer to the highest height of a point intersected in the plant canopy (even if it was the middle of a branch or stem which extended laterally and vertically). Maximum shrub height was the highest point of vegetation within 1 meter on either side of the transect recorded within vegetation communities along each transect as defined by Walker and Bockheim (1995). Maximum shrub heights were not recorded at Flux 1, 2, or 4. Flux 1 and 2 were omitted in 1995 due to the paucity of shrubs present in the plot at the time; Flux 4 was not sampled, perhaps due to time constraints. Cloud-based vegetation measurements were summarized by site and compared to both 1995 mid canopy heights and 1995 maximum shrub heights.

3.3 Results

3.3.1 Quantitative Assessment of Canopy Heights from the Agisoft Workflow

Canopy height estimates from Agisoft's standard workflow included numerous negative values at all sites (Figure 7). The estimates of canopy heights were similar at each plot, which did not reflect the true variation in heights measured at each site. The auto-classification of dense cloud points used parameters that were not designed to work with vegetation less than 0.5 m, which is what grows in most of these tundra plots (Agisoft Helpdesk Portal, 2022).

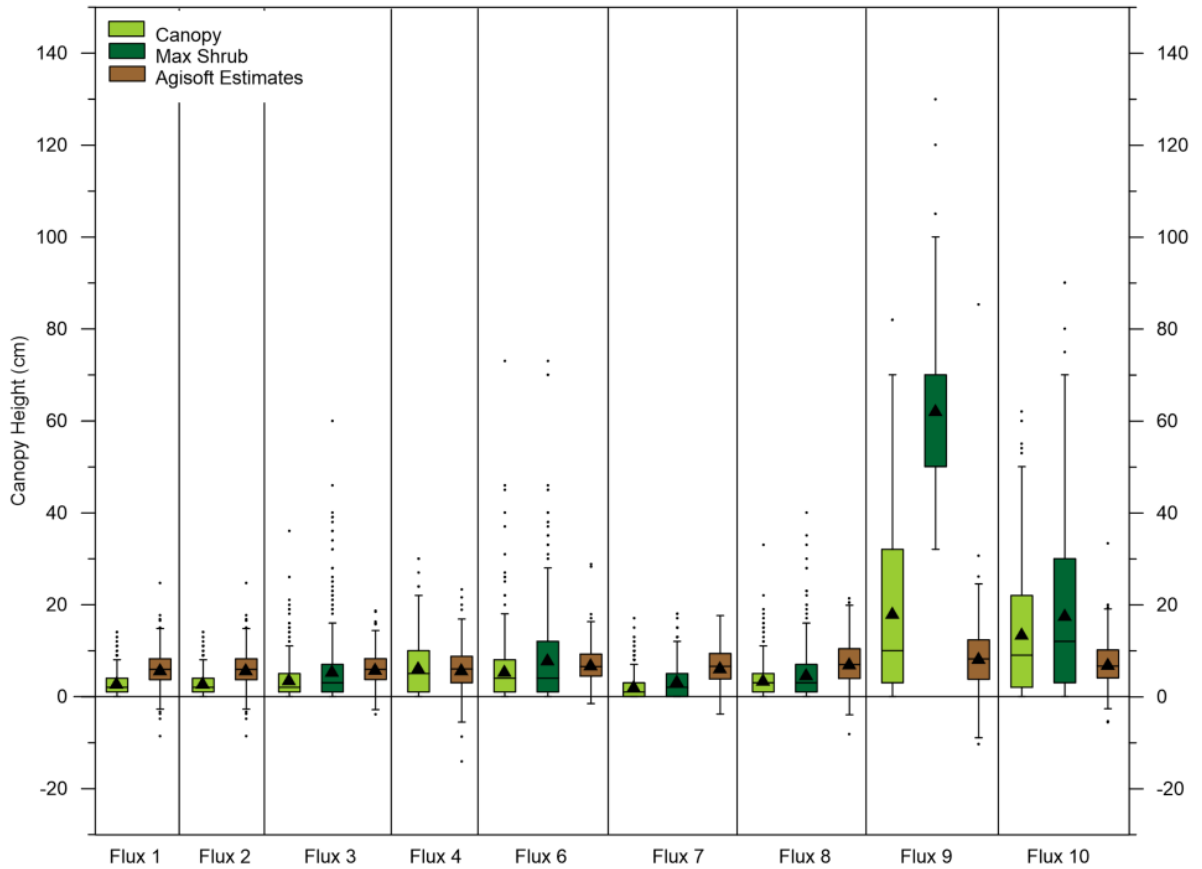


Figure 7: Boxplots (quartiles and median) showing cloud-based estimates of canopy heights using Agisoft standard procedures, and 1995 field measurements of canopy heights and maximum shrub heights. Mean values marked by triangles.

3.3.2 Spatial and Qualitative Assessment of Canopy Heights from the lidR Workflow

Results from lidR classification include DTM, DSM, and CHMs mapped for visual assessment and assessed qualitatively. In the next section canopy heights extracted along the Plot transects were evaluated quantitatively. Figures 8 – 16 show a selection of resulting DTMs at 0.1 m and 1.0 m, DSMs at 0.1 m and 1.0 m, and CHMs generated using resolutions of 0.1 m (DSM) / 0.1 m (DTM), 0.25 m (DSM) / 1.0 m (DTM), and 1.0 m (DSM) / 1.0 m (DTM).

Flux 1

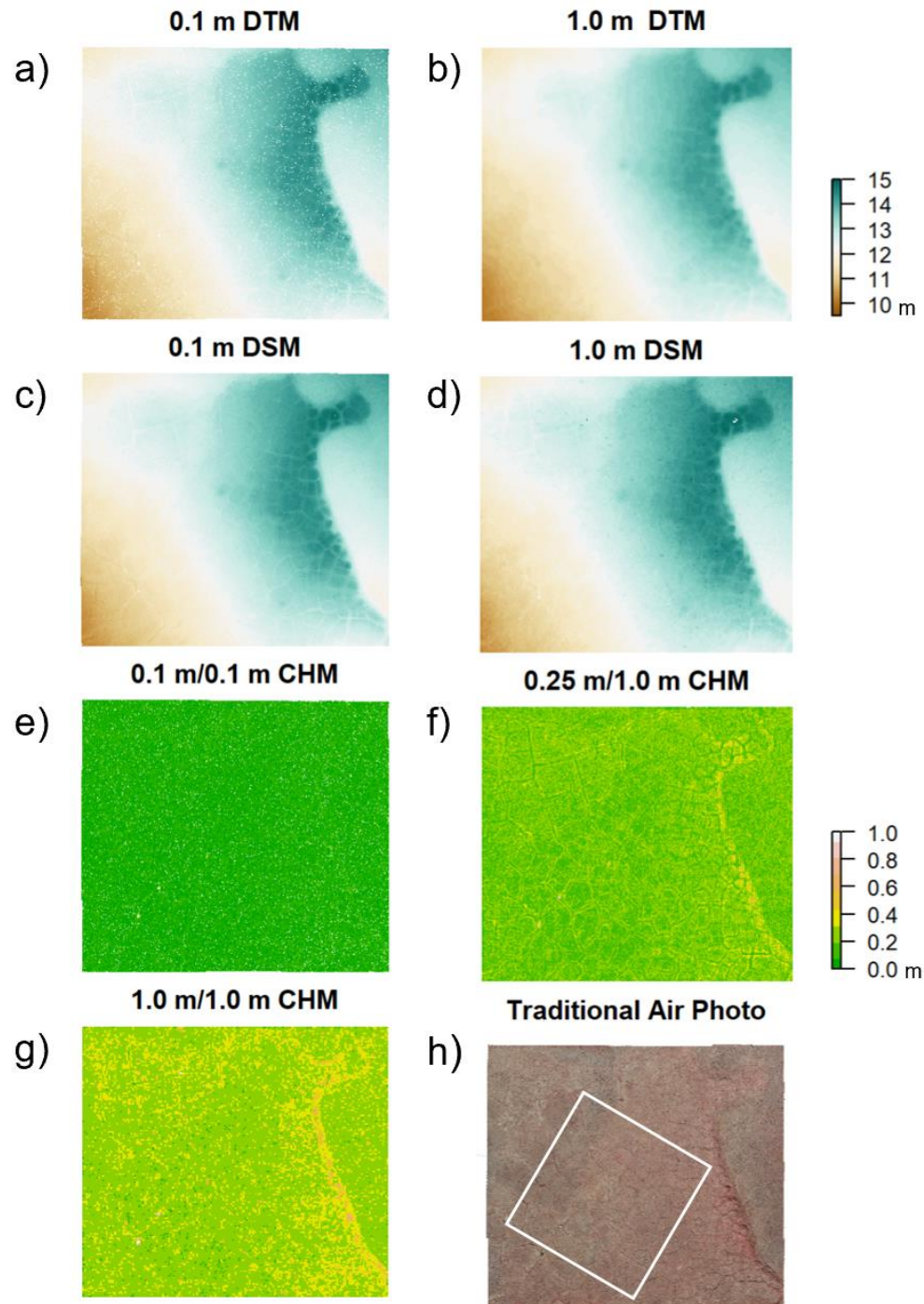


Figure 8: Maps of Flux Plot 1. Digital terrain models (DTM) at (a) 0.1 m and (b) 1.0 m, digital surface models (DSM) at (c) 0.1 m and (d) 1.0 m, and canopy height models of the difference between the DSM and DTM at (e) 0.1 and 0.1 m resolution, respectively, (f) at 0.25 m and 1.0 m and (g), at 1.0 and 1.0 m, and (h) a portion of one of the 1995 aerial photos with a white square indicating the boundaries of the 100 × 100 m plot.

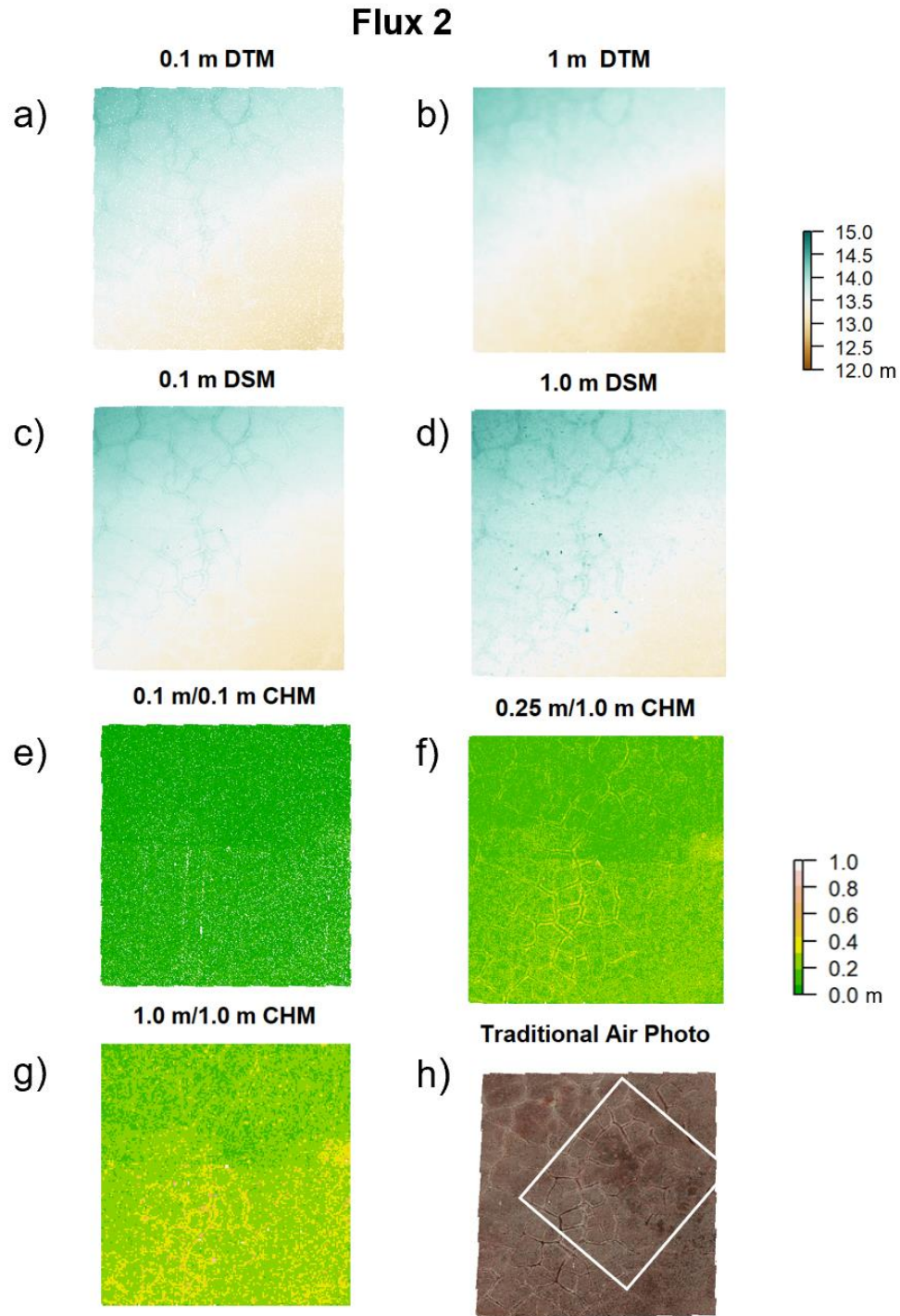


Figure 9: Maps of Flux Plot 2. Digital terrain model (DTM) at (a) 0.1 m and (b) 1.0 m, digital surface model (DSM) at (c) 0.1 m and (d) 1.0 m, and canopy height models of the difference between the DTM and DSM at (e) 0.1 and 0.1 m resolution, respectively, (f) at 0.25 m and 1.0 m and (g), at 1.0 and 1.0 m, and (h) a portion of a traditional aerial photo with a white square indicating the boundaries of the 100 x 100 m plot.

Flux 3

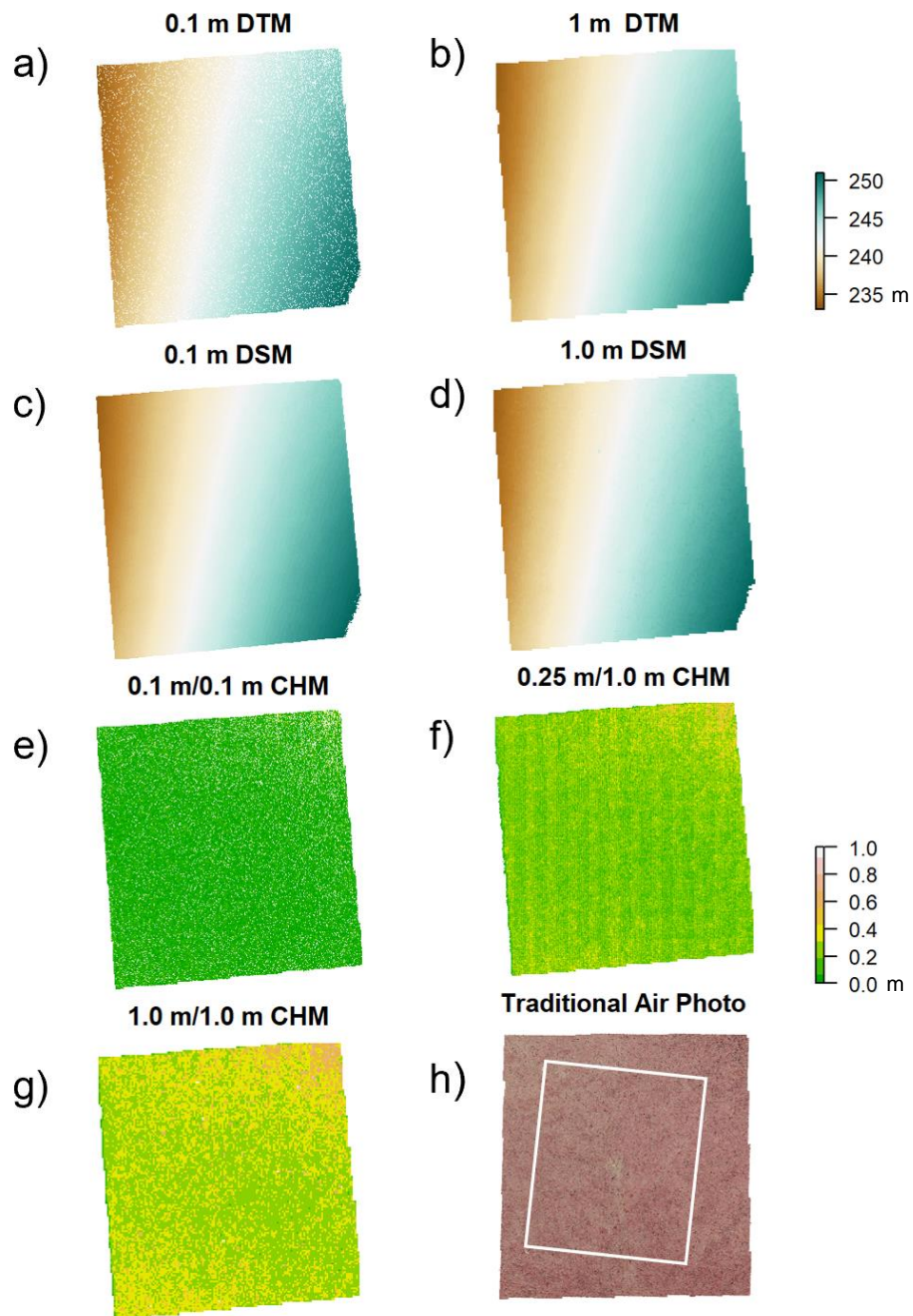


Figure 10: Maps of Flux Plot 3. Digital terrain model (DTM) at (a) 0.1 m and (b) 1.0 m, digital surface model (DSM) at (c) 0.1 m and (d) 1.0 m, and canopy height models of the difference between the DTM and DSM at (e) 0.1 and 0.1 m resolution, respectively, (f) at 0.25 m and 1.0 m and (g), at 1.0 and 1.0 m, and (h) a portion of a traditional aerial photo with a white square indicating the boundaries of the 100 x 100 m plot.

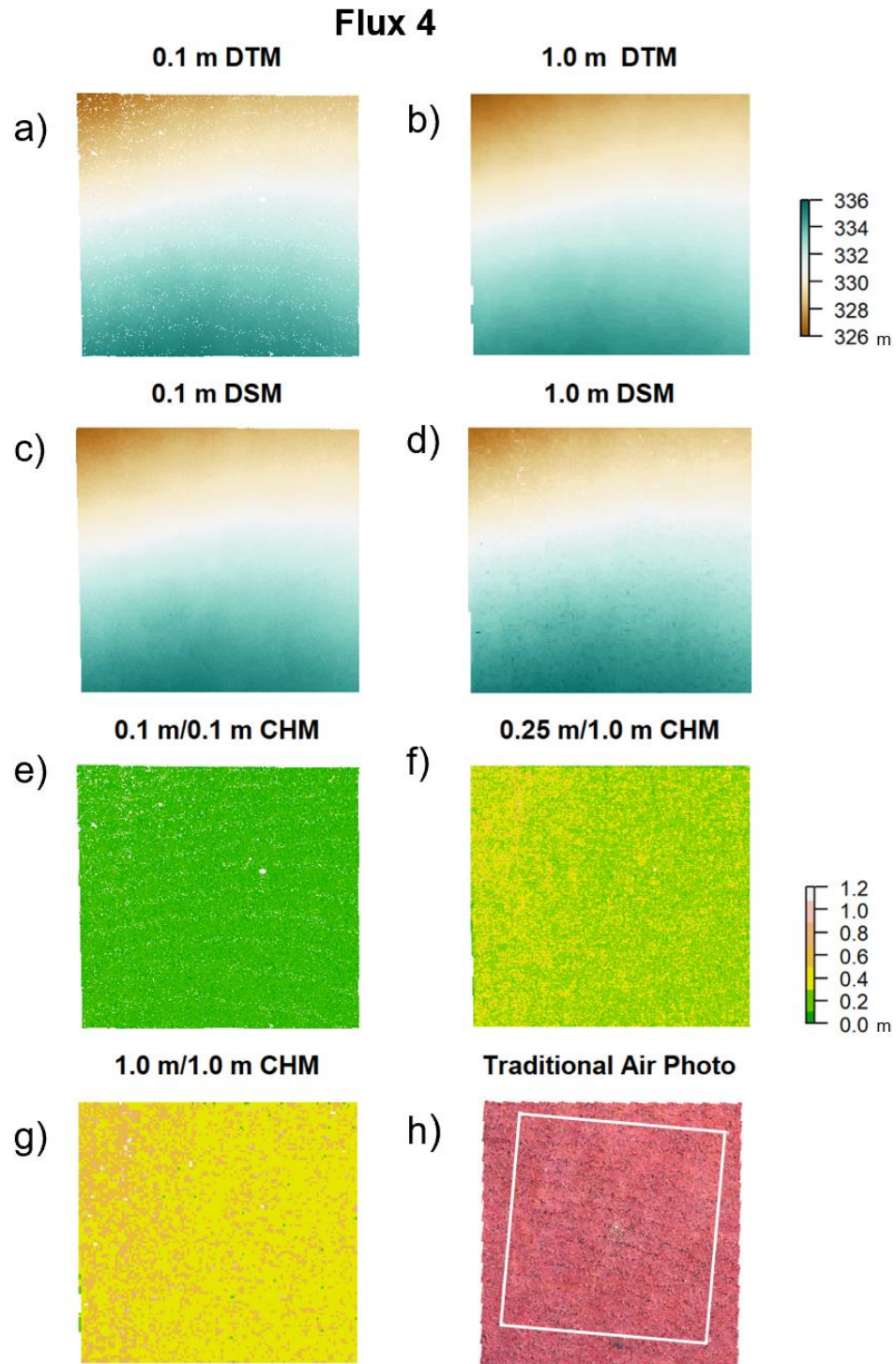


Figure 11: Maps of Flux Plot 4. Digital terrain model (DTM) at (a) 0.1 m and (b) 1.0 m, digital surface model (DSM) at (c) 0.1 m and (d) 1.0 m, and canopy height models of the difference between the DTM and DSM at (e) 0.1 and 0.1 m resolution, respectively, (f) at 0.25 m and 1.0 m and (g), at 1.0 and 1.0 m, and (h) a portion of a traditional aerial photo with a white square indicating the boundaries of the 100 x 100 m plot.

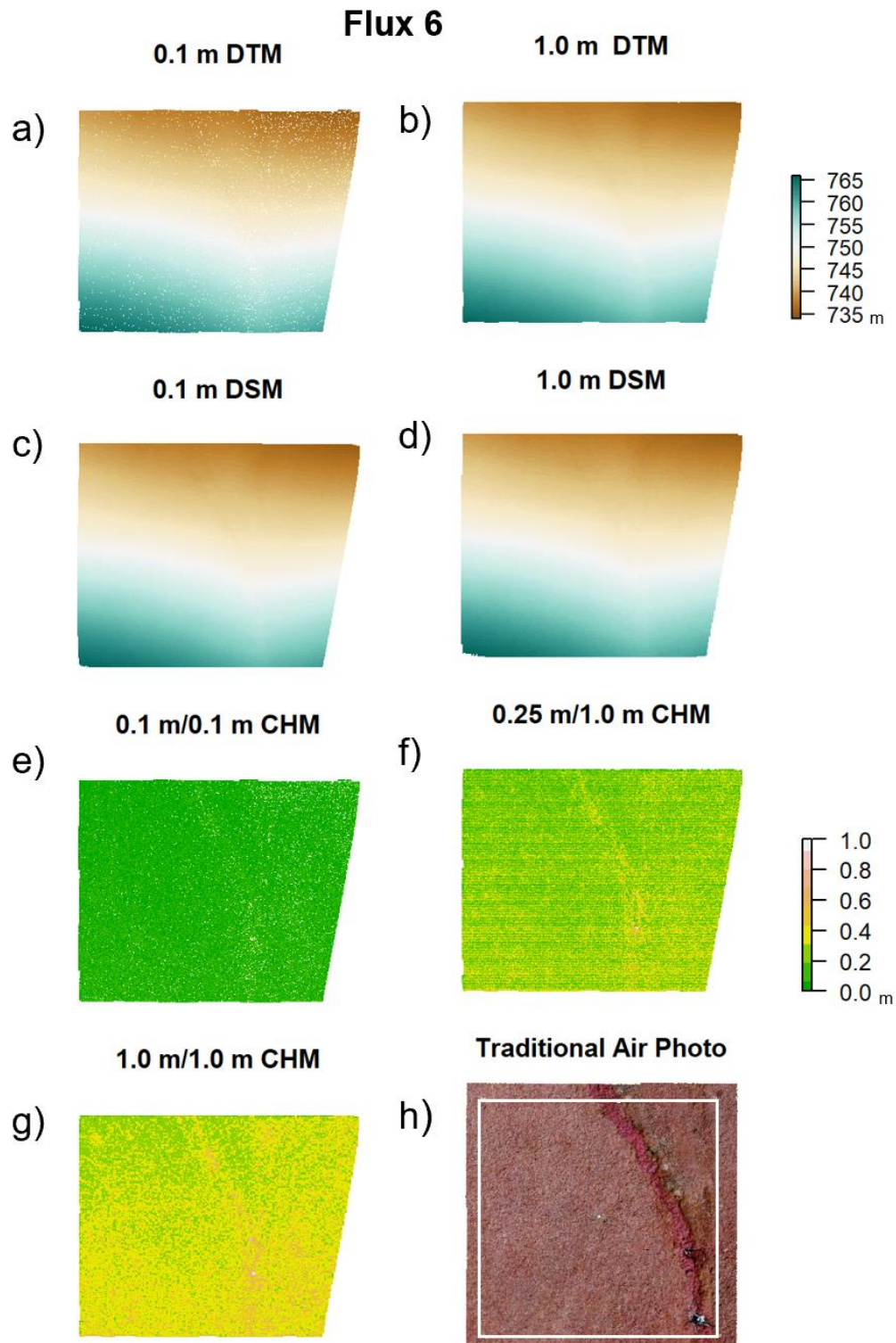


Figure 3: Maps of Flux Plot 6. Digital terrain model (DTM) at (a) 0.1 m and (b) 1.0 m, digital surface model (DSM) at (c) 0.1 m and (d) 1.0 m, and canopy height models of the difference between the DTM and DSM at (e) 0.1 and 0.1 m resolution, respectively, (f) at 0.25 m and 1.0 m and (g), at 1.0 and 1.0 m, and (h) a portion of a traditional aerial photo with a white square indicating the boundaries of the 100 x 100 m plot.

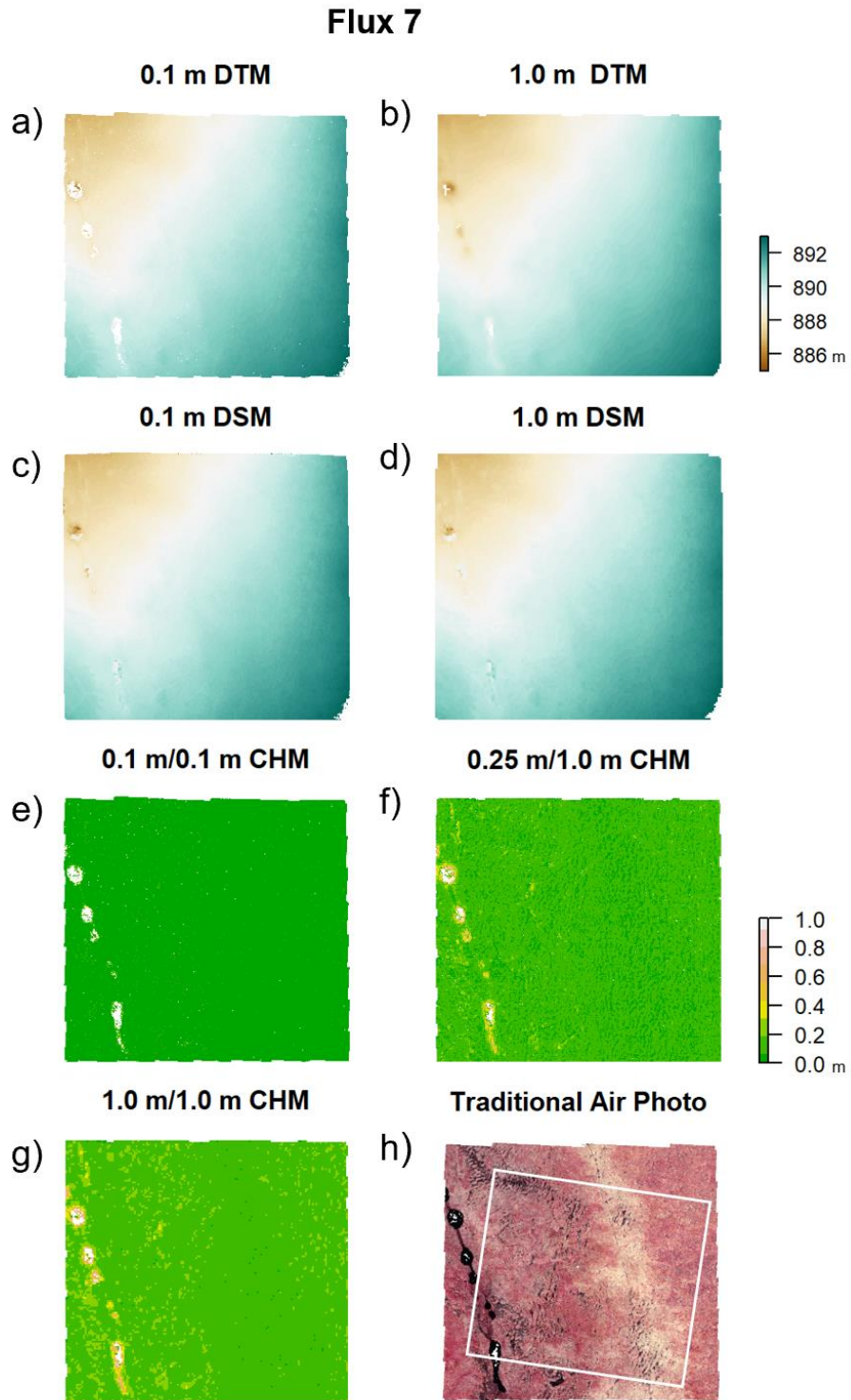


Figure 4: Maps of Flux Plot 7. Digital terrain model (DTM) at (a) 0.1 m and (b) 1.0 m, digital surface model (DSM) at (c) 0.1 m and (d) 1.0 m, and canopy height models of the difference between the DTM and DSM at (e) 0.1 and 0.1 m resolution, respectively, (f) at 0.25 m and 1.0 m and (g), at 1.0 and 1.0 m, and (h) a portion of a traditional aerial photo with a white square indicating the boundaries of the 100 x 100 m plot.

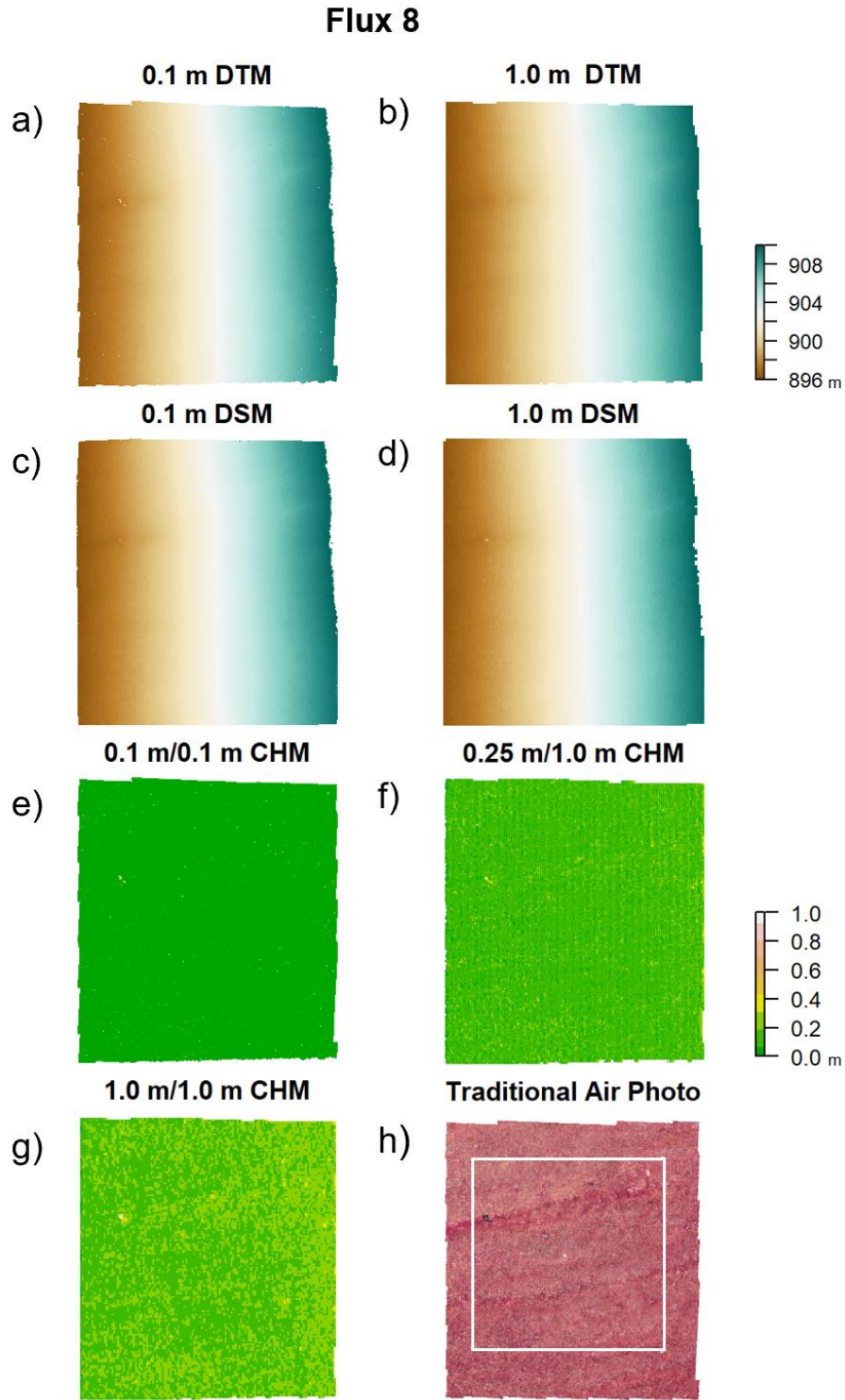


Figure 5: Maps of Flux Plot 8. Digital terrain model (DTM) at (a) 0.1 m and (b) 1.0 m, digital surface model (DSM) at (c) 0.1 m and (d) 1.0 m, and canopy height models of the difference between the DTM and DSM at (e) 0.1 and 0.1 m resolution, respectively, (f) at 0.25 m and 1.0 m and (g), at 1.0 and 1.0 m, and (h) a portion of a traditional aerial photo with a white square indicating the boundaries of the 100 x 100 m plot.

Flux 9

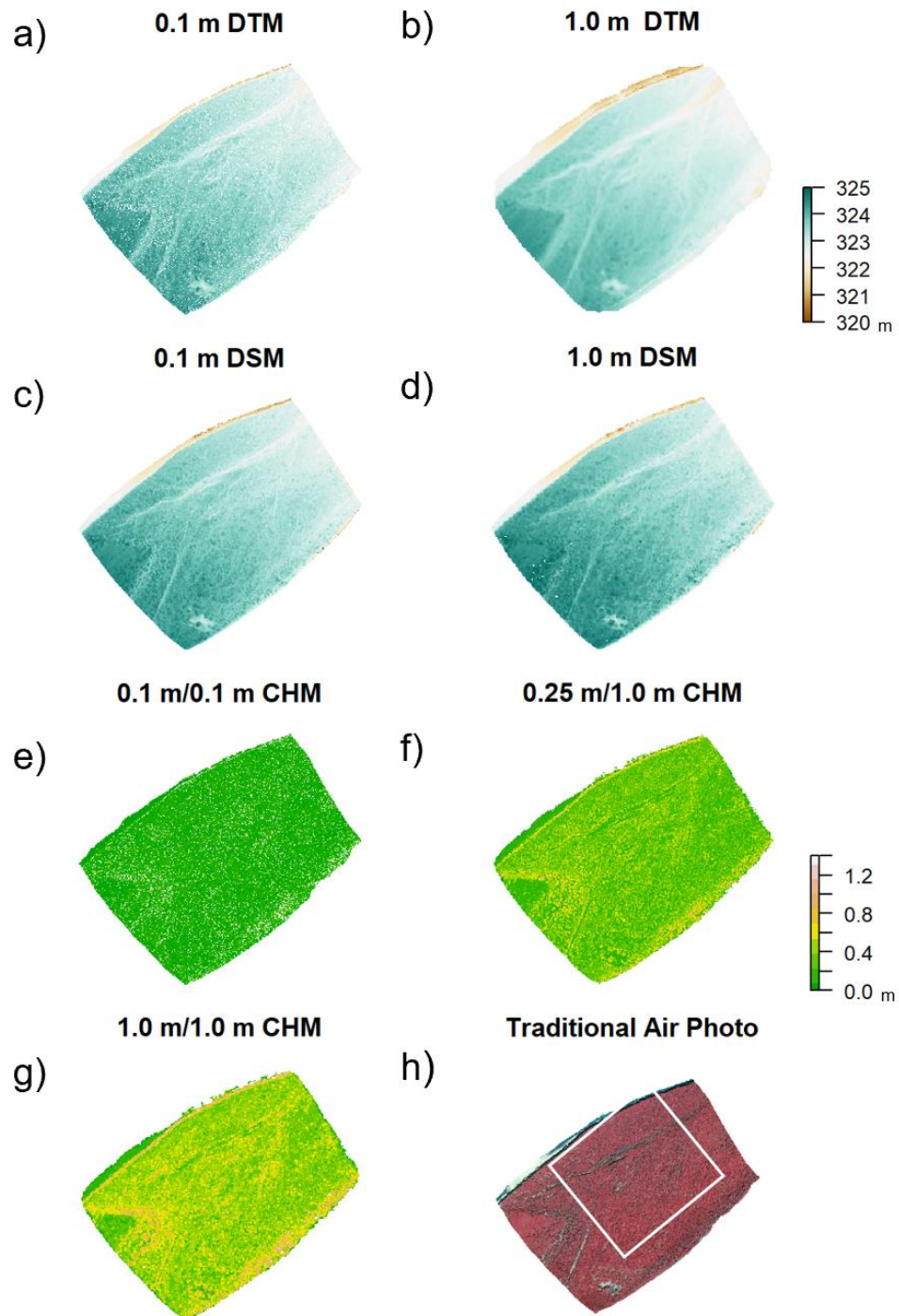


Figure 6: Maps of Flux Plot 9. Digital terrain model (DTM) at (a) 0.1 m and (b) 1.0 m, digital surface model (DSM) at (c) 0.1 m and (d) 1.0 m, and canopy height models of the difference between the DTM and DSM at (e) 0.1 and 0.1 m resolution, respectively, (f) at 0.25 m and 1.0 m and (g), at 1.0 and 1.0 m, and (h) a portion of a traditional aerial photo with a white square indicating the boundaries of the 100 x 100 m plot.

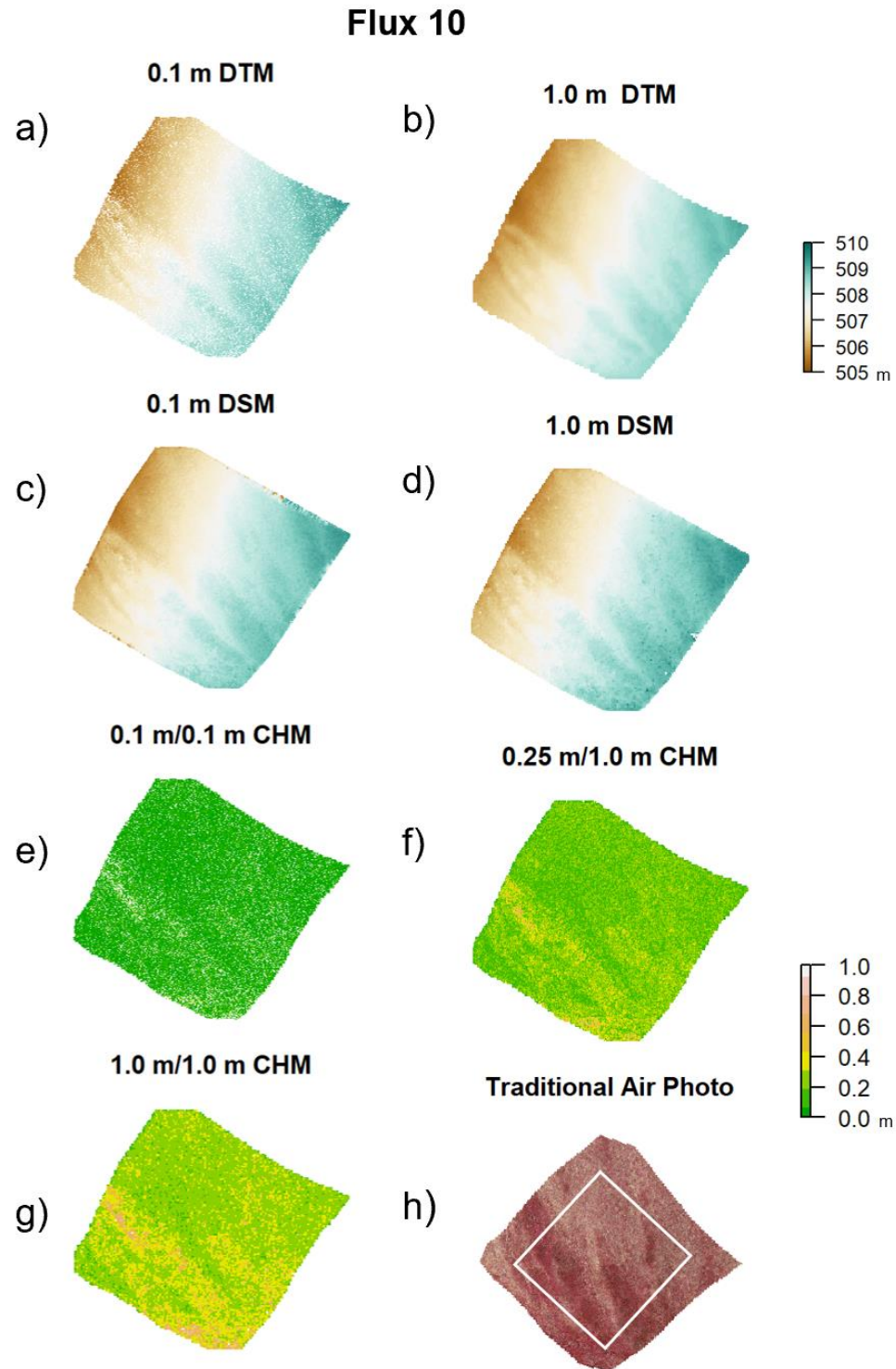


Figure 7: Maps of Flux Plot 10. Digital terrain model (DTM) at (a) 0.1 m and (b) 1.0 m, digital surface model (DSM) at (c) 0.1 m and (d) 1.0 m, and canopy height models of the difference between the DTM and DSM at (e) 0.1 and 0.1 m resolution, respectively, (f) at 0.25 m and 1.0 m and (g), at 1.0 and 1.0 m, and (h) a portion of a traditional aerial photo with a white square indicating the boundaries of the 100 x 100 m plot.

Due to the topography and short vegetation heights at these plots, some features may not be visible until subtracted in the CHMs. DSMs and DTMs were not slope corrected.

Visual evaluation of DTM, DSM, and CHM maps confirmed that most expected in-situ geomorphic features, such as ice wedge polygons at Flux 1 and 2 (Figures 8 and 9), beaded-stream ponds at Flux 7 (Figure 13), and linear erosion features at Flux 9 (Figure 15) could be identified. The taller vegetation in the water tracks was visible on the CIR traditional aerial photos at Flux 6, 8, and 10 (h in Figures 12, 14, and 16). These features are also visible on the CHM maps, with coarser resolutions (e.g. 1.0/1.0) maps appearing to show maximum height most clearly (g in Figures 12, 14, and 16).

The finest resolution DSM, DTM, and CHM maps (c, e, and g in Figures 8-16) have the most missing pixels, as expected. They also do not visibly show the full variability of heights present in the plots. As resolution coarsens, there are fewer missing pixels and taller maximum shrub heights become more apparent. However, at coarser resolutions it appears that the CHMs have very few pixels of short vegetation. CHM maps with mixed (0.25/1.0) and coarser (1.0/1.0) resolutions appear to capture more of the variability in canopy heights than at either the finest (0.1/0.1) resolutions. Results from 2.0/2.0 are not shown but continued the trends.

3.3.3 Quantitative Assessment of Canopy Heights from the lidR Workflow

Box-plots of the measured canopy heights, maximum shrub heights, and the cloud-based estimates provide quantitative comparisons at a series of spatial resolutions (Figure 17). Information about the DSM and DTM layers was also revealed. Estimated mean point-cloud heights were plotted against measured canopy heights (Figure 18) and maximum shrub heights (Figure 19). One-way ANOVA tests were used to compare the mean values of CHMs with mean field measured canopy heights (Table 9) and maximum shrub mean heights (Table 10).

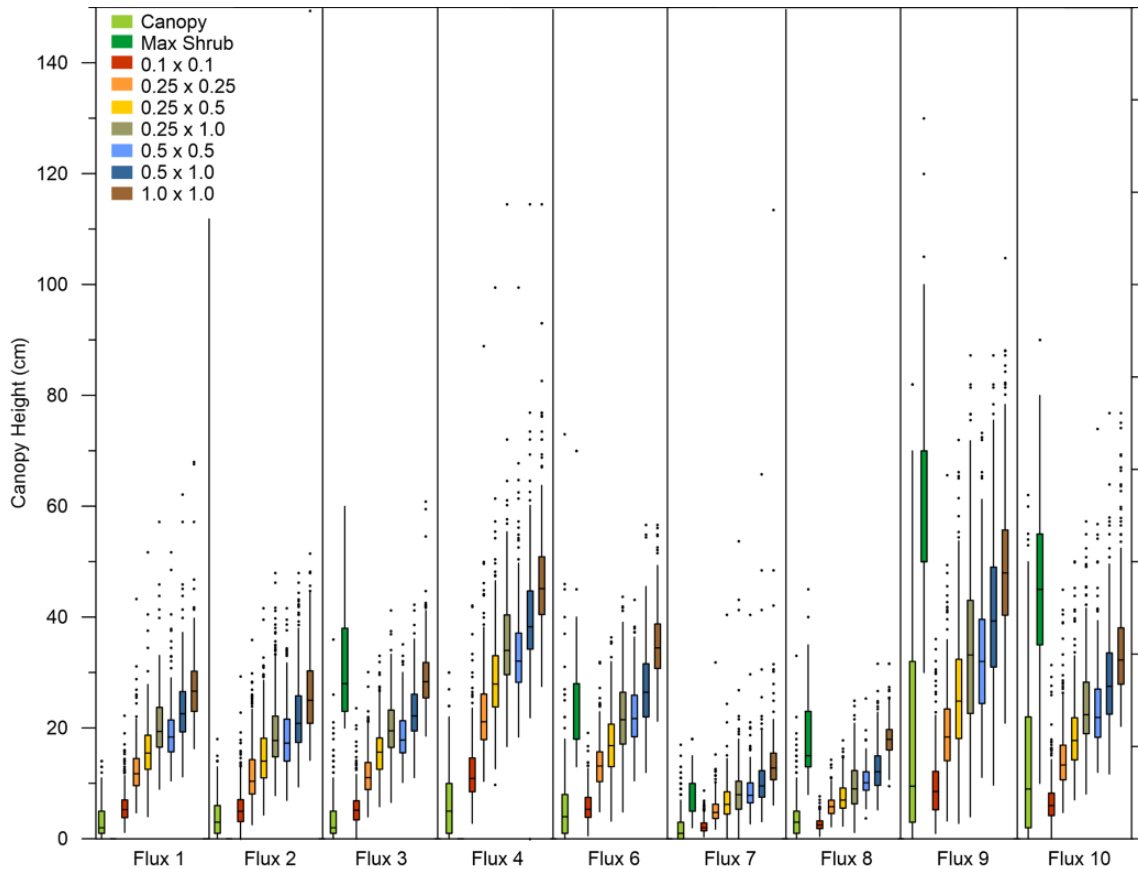


Figure 8: Boxplots (quartiles and medians) of canopy height and maximum shrub height field measurements in 1995 and point-cloud estimates of vegetation height at varying CHM (DSM/DTM; m/m) resolutions.

At the finest resolution of 0.1/0.1, minimum canopy heights were closest to those observed at all sites (Figure 17). No negative canopy height values were calculated along the transects using the lidR algorithms as compared to the Agisoft workflow. The mixed resolution (0.25/1.0 and 0.5/1.0) CHMs showed that having a finer resolution DSM helped to maintain a more accurate minimum value even while coarsening the DTM. Examined individually (not shown), DTM minimum elevations did not change systematically, but the DSMs minimum elevations substantially increased with coarsening, resulting in fewer short estimates of canopy heights (Figure 17).

As CHM resolution increased, median canopy heights also increased (Figure 17). A CHM resolution of 2.0/2.0 (not shown) estimated higher medians than a CHM at 1.0/1.0 m.

Estimated CHM means were closer to measured canopy heights at the finer resolutions (0.1/0.1 and 0.25/0.25) for all sites but Flux 4, with differences within ± 2.8 cm (Figure 18 and Table 9). The photos used for photogrammetry analysis at Flux 4 were taken such that the plot was not near the center which likely reduced accuracy. The ANOVA tests (Table 9) show the difference between observed canopy heights and CHM predicted values. These results indicate CHM means were within 0.1 cm of expected at the 0.1/0.1 resolution for Flux 6 and 7, and within 1.3 cm at 0.25/0.25 resolution for Flux 9 and 10. The remaining results show statistically significant differences between the observed canopy heights and predicted CHMs. As resolution increased, photogrammetrically-estimated heights overestimated observed heights; however, CHMs performed better with a finer pixel resolution.

Observed maximum canopy height values were often several times the mean canopy height, with very few observations. Cloud-based CHM maximums were often underestimated as well as overestimated compared to the field measurements, although coarser resolution CHMs systematically predicted taller values (Figure 17).

In summary, as pixel resolution increased, CHM estimates also increased. When compared to in-situ canopy height measurements, finer resolution CHMs outperformed coarse resolution CHMs.

3.3.4 Quantitative Assessment of Maximum Shrub Heights from the lidR Workflow

Other studies have compared maximum shrub heights to cloud-based canopy heights, so we also compared CHM values to field observations of maximum shrub heights at the five plots which were measured in 1995.

When minimum values of maximum shrub heights were compared to minimum CHMs, coarser resolution CHMs yielded estimates closer to observed values than the finer resolution CHMs, but not reliably (Figure 17).

Observed medians of CHMs consistently increased with coarser resolution. However even the coarsest cloud-based (1.0/1.0) CHMs were not systematically related to median maximum shrub heights; observed median maximum shrub heights were underestimated at Flux 9 and 10, within a few cm at Flux 3 and 8, and overestimated at Flux 6.

Mean point-cloud CHM estimates more often underestimated mean observed maximum shrub heights (Figure 19 and Table 10). At Flux 8, the estimated mean CHM value at 1.0/1.0 resolution was equal to the observed CHM height. Flux 7 CHM estimates at 0.25/0.5 were within 0.5 cm of the observed mean maximum shrub value, and Flux 6

estimates at 0.25/1.0 and 0.5/0.5 also performed well (Figure 19 and Table 10). The remaining ANOVA tests showed statistically significant differences between CHM values and field measurement. Coarser resolution (1.0/1.0) CHMs seem to more accurately capture mean maximum shrub heights than finer resolution CHMs.

CHM maximum values tended to underestimate maximums of the maximum shrub field measurements (Figure 17), although coarser resolution generally had closer estimates than finer resolution CHMs. In some cases (Flux 7 and 3), CHMs overestimated field measurements which may be due to noise.

Overall, the results from this study show that finer resolution CHMs appear to be capturing canopy height measurements more accurately than maximum shrub heights.

Generally, coarser resolution CHMs produce taller estimates than finer resolution CHMs.

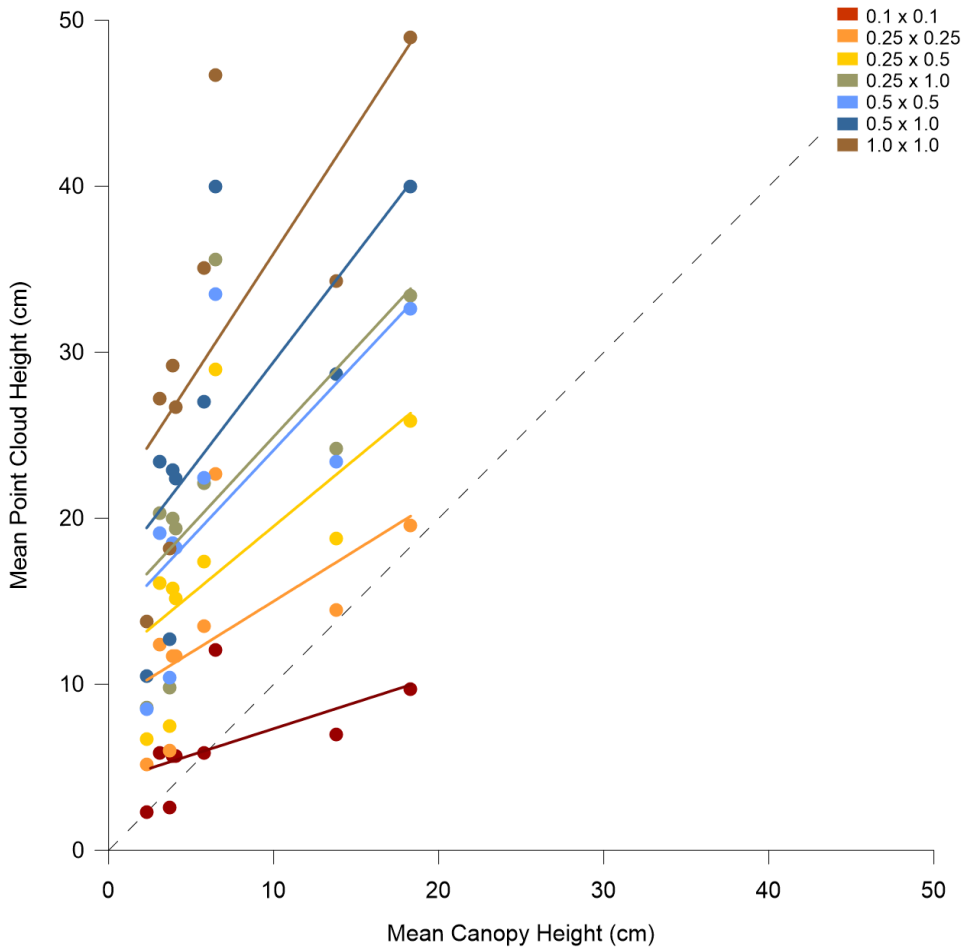


Figure 9: Mean canopy heights compared to mean point cloud estimates at varying resolution. Each point represents 340 observations summarized by plot. Points are ordered from shortest to tallest site (Flux Plots 7, 1, 8, 3, 2, 6, 4, 10 and 9, respectively). Linear regressions are shown for each resolution. The dotted line represents the 1:1 relationship for reference.

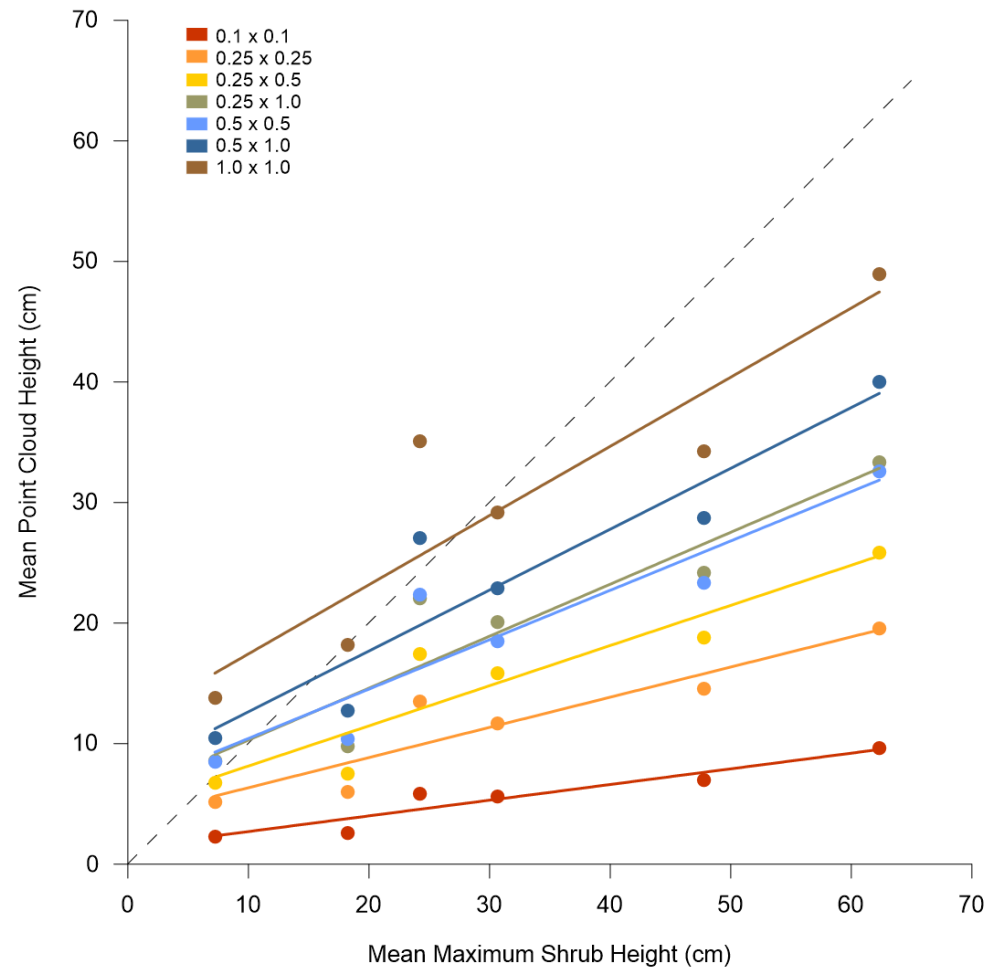


Figure 10: Mean maximum shrub heights compared to mean point cloud canopy height estimates at varying resolution. Each point represents 25-90 field observations (see Table 3 for complete list of sites with maximum shrub heights collected in 1995) and 340 point cloud estimates, all summarized by plot. Points are ordered from shortest to tallest site (Flux Plots 7, 8, 6, 3, 10 and 9, respectively). The dotted line represents the 1:1 relationship for reference.

Site	Measured mean canopy heights (cm)	Estimated CHM means at varying DSM/DTM (m/m) resolutions (cm)						
		0.1/0.1	0.25/0.25	0.25/0.5	0.25/1.0	0.5/0.5	0.5/1.0	1.0/1.0
Flux 7	2.3	2.3	5.2	6.7	8.6	8.5	10.5	13.8
p value		0.9	3.3E-33	8.1E-51	2.7E-60	1.3E-89	7.1E-87	4.3E-104
Flux 1	3.1	5.9	12.4	16.1	20.3	19.1	23.4	27.2
p value		4.7E-29	5.2E-138	4.8E-179	3.6E-221	5.1E-220	5.5E-250	7.7E-287
Flux 8	3.7	2.6	6	7.5	9.8	10.4	12.7	18.2
p value		1.8E-06	4.9E-19	1.8E-40	1.9E-62	8.6E-101	5.0E-117	2.7E-240
Flux 3	3.9	5.7	11.7	15.8	20	18.5	22.9	29.2
p value		2.6E-09	4.4E-92	3.1E-147	1.9E-190	2.4E-194	2.6E-233	4.0E-289
Flux 2	4.1	5.7	11.7	15.2	19.4	18.2	22.4	26.7
p value		1.5E-07	1.7E-80	2.9E-123	3.4E-162	1.4E-160	3.9E-190	1.0E-173
Flux 6	5.8	5.9	13.5	17.4	22.1	22.4	27	35.1
p value		0.8	3.4E-51	6.3E-83	5.9E-118	3.9E-142	1.3E-168	2.0E-250
Flux 4	6.5	12.1	22.7	29	35.6	33.5	40	46.7
p value		2.6E-29	2.8E-122	3.6E-166	3.2E-206	2.7E-207	4.1E-236	4.3E-271
Flux 10	13.8	7	14.5	18.8	24.2	23.4	28.7	34.3
p value		1.8E-15	0.4	3.7E-09	9.0E-30	2.3E-26	2.5E-53	1.8E-81
Flux 9	18.3	9.7	19.6	25.9	33.4	32.6	40	49
p value		3.3E-13	0.3	1.1E-09	3.9E-27	8.6E-29	8.3E-52	8.4E-92

Table 8: One-way ANOVA results showing measured mean canopy heights (cm) and estimated mean CHMs (cm) at varying DSM/DTM (m/m) resolutions. P-values > 0.05 are in bold, indicating similar group means. Table is arranged by mean height at each plot, from smallest to largest.

Site	Measured Max Shrub Mean (cm)	Estimated CHM means at varying DSM/DTM (m/m) resolutions (cm):						
		0.1/0.1	0.25/0.25	0.25/0.5	0.25/1.0	0.5/0.5	0.5/1.0	1.0/1.0
Flux 7	7.2	2.3	5.2	6.7	8.6	8.5	10.5	13.8
p value		3.0E-64	2.8E-09	0.3	0.0	0.0	3.1E-07	2.0E-15
Flux 8	18.2	2.6	6.0	7.5	9.8	10.4	12.7	18.2
p value		5.1E-99	1.1E-62	8.9E-43	3.7E-18	2.2E-26	1.4E-09	0.95
Flux 6	24.2	5.9	13.5	17.4	22.1	22.4	27.0	35.1
p value		6.3E-79	6.6E-29	3.9E-10	0.1	0.1	0.0	6.4E-21
Flux 3	30.6	5.7	11.7	15.8	20.0	18.5	22.9	29.2
p value		2.4E-94	6.4E-61	1.8E-35	7.4E-17	1.3E-27	9.5E-11	2.5E-01
Flux 10	47.8	7.0	14.5	18.8	24.2	23.4	28.7	34.3
p value		6.5E-119	3.4E-89	1.4E-68	2.0E-45	1.1E-49	8.9E-31	1.7E-14
Flux 9	62.4	9.7	19.6	25.9	33.4	32.6	40.0	49.0
p value		2.0E-106	1.1E-73	3.3E-45	1.3E-22	7.8E-33	1.1E-15	2.2E-07

Table 9: One-way ANOVA results showing measured mean maximum shrub heights (cm) and estimated mean CHMs (cm) at varying DSM/DTM (m/m) resolutions. P-values > 0.05 are in bold, indicating similar group means. Table is arranged by mean heights at each plot, from smallest to largest.

3.4 Discussion

One of the main challenges in tundra ecological monitoring is finding scale-appropriate observations due to the small-statured nature of vegetation over this immense and remote area (Greaves et al., 2019). This study aimed to fill an important scale gap between satellite remote sensing studies and in-situ observations by utilizing a fine-scale remote sensing approach. By pairing a modern photogrammetry workflow with point clouds derived from traditional aerial photos, we found that estimated tundra canopy heights consistently increased as pixel resolution increased. This study demonstrates the inherent challenges associated with differences in data acquisition and processing of short vegetation with structural complexity and high spatial heterogeneity (Fraser et al., 2016).

3.4.1 Data Acquisition and Processing

Flying height, shadowing effects, image overlap, and geometry can all impact CHM accuracy (Liu et al., 2020). Here, a standard photogrammetry image processing workflow and LiDAR-based classification were utilized with the traditional photos to generate CHMs. While imagery used in this study was finer than typical traditional aerial photography (7 cm in 1995), it was acquired with a flying height (1,500 feet) much higher than used with UAVs (though low for traditional air photos), limited GCPs, traditional image overlap, and a nadir-pointing camera. The lack of vertical control in an area with seasonal heave and subsidence could have introduced more distortion. All of these limitations in data collection and processing likely influenced CHM results. Point-cloud generation using Agisoft Metashape seemed to perform well for our application. However, auto-classification of points for CHM generation is not standardized to work in

an environment where vegetation is <1 m tall (Agisoft Helpdesk Portal, 2022), so we then tested the utility of alternate software.

While the *lidR* package was primarily developed to process airborne laser scanning (ALS) data, it is capable of handling alternate sources of point clouds including photogrammetry (Roussel et al., 2020). Several studies have successfully used *lidR* to process UAV point clouds (Navarro et al., 2020, Van Valkenburgh et al., 2020), yet none had used point clouds derived from traditional aerial photos.

Photogrammetry is generally limited to depiction of the outer canopy surface because passive sensor-based point clouds contain little information on sub-canopy vegetation or terrain in areas with dense canopy cover (Lisein et al., 2013). Penetration through the canopy to the ground and accurate DTM generation is difficult to achieve in environments where vegetation is characterized by continuous cover and few patches of true bare ground. Furthermore, surveys with less image overlap have fewer observations of shadowed ground features within the gaps of individual shrubs, making reconstruction of bare earth models more difficult (Fraser et al., 2016). One way to overcome this issue is by using terrain-filtering algorithms (Lisein et al., 2013) as is done within *lidR*, assuming that true ground points are found within the point cloud.

3.4.2 Interpolation and Pixel Resolution

Optimizing grid resolution and the choice of interpolation algorithms are essential to accurately mapping both ground and vegetation surfaces (Vepakomma et al., 2008). Point-cloud density has a significant effect on DSM and DTM accuracy (Cao et al., 2019). While photogrammetry results in high point-cloud density, choice of grid resolution has a strong influence on the errors introduced during interpolation

(Vepakomma et al., 2008). A larger cell size results in more points per pixel than a smaller cell size. A fine spatial resolution can have void cells, while a coarse resolution will contain points within each cell which will not be utilized, presenting a tradeoff for determining optimal spatial resolution (Vepakomma et al., 2008). In this study, increasing pixel resolution led to increasing estimates of tundra canopy heights (Figure 17). This indicated that as point cloud density decreased, there was a decrease in accuracy of canopy height estimates. The finer resolution CHMs (0.1/0.1 and 0.25/0.25) performed better when compared to lower canopy heights, and coarser resolution CHMs (1.0/1.0) seem to work better with taller canopy heights. The DSMs may be driving this result, as minimum elevations substantially increased with coarsening pixel resolution, and led to shorter canopy height estimates. Other studies have found that detailed canopy structures tend to be suppressed at coarse resolution (Liu et al., 2020).

Choices in interpolation algorithms and numerous parameters during CHM workflow impacted the CHMs. The algorithms generally found the minimum value point to generate the DSM, and the maximum value point to generate the DTM. One objective of this study was to see if CHMs could more reliably capture mid canopy or maximum canopy measurements. Upon comparison, we found that point-cloud measurements generally overestimated canopy heights and underestimated maximum heights, and that increasing resolution increased overall height estimates. In a forest study of deciduous trees up to 30 m tall, Liu et al. (2020) tested spatial resolutions between 0.1 and 1.0 m and found similar results where photogrammetry tended to overestimate low canopy heights and underestimate high canopy heights. Another study in the Canadian Arctic reported good correspondence between UAV-derived canopy heights (< 1m) and in-situ

maximum canopy heights (Clement and Fraser, 2017). However, inherent sensitivities associated with differences in data collection and processing are difficult to summarize (Cunliffe et al., 2020).

3.5 Conclusion

This study explored the utility of traditional air photos to measure vegetation canopy heights on the North Slope of Alaska. We applied a modern photogrammetry workflow to process point clouds and a LiDAR-based classification to generate CHMs. When compared to field measurements, mean point-cloud estimated canopy heights calculated at 10 cm resolution showed differences of 0 to 2.8 cm at sites with measured mean canopy heights between 2.3 and 5.8 cm (Plots 1, 2, 3, 6, 7, and 8). At sites with taller vegetation (mean canopy heights of 13.8 and 18.5 cm; Plots 10 and 9) differences were just 0.7 and 1.6 cm, respectively, from point-cloud estimates made at 0.25 cm resolution. and underestimated maximum heights. Finer resolution CHMs work better when compared to lower canopy heights, and coarser resolution CHMs work better with taller canopy heights. These results suggest that fine-scale remote sensing techniques can perform well to estimate canopy heights for tundra vegetation with and without dwarf shrubs. Further studies are necessary to improve our understanding of the impacts of pixel resolution, fine-scale remote sensing data acquisition and point cloud processing, and on canopy height estimates. This may aid in the quantification of long-term vegetation change and response to amplified warming on the North Slope of Alaska.

APPENDIX:

Top of Plant Canopy Percent Cover

Functional Group	Flux 3: 1995	Flux 3: 2021	Flux 4: 1995	Flux 4: 2021	Flux 6: 1995	Flux 6: 2021	Flux 7: 1995	Flux 7: 2021	Flux 8: 1995	Flux 8: 2021	Flux 10: 1995	Flux 10: 2021
Bryophyte	25.0	3.6	25.9	3.6	14.3	7.1	46.4	7.4	25.9	14.3	17.9	7.4
Deciduous	0.0	17.9	14.8	14.3	25.0	35.7	17.9	22.2	18.5	32.1	60.7	55.6
Evergreen	28.6	28.6	7.4	7.1	32.1	10.7	3.6	3.7	18.5	17.9	0.0	3.7
Forb	0.0	7.1	3.7	10.7	0.0	0.0	0.0	0.0	11.1	0.0	0.0	7.4
Graminoid	39.3	42.9	40.7	60.7	10.7	39.3	14.3	51.9	11.1	32.1	14.3	18.5
Lichen	0.0	0.0	0.0	3.6	3.6	0.0	0.0	0.0	0.0	0.0	0.0	0.0
Litter	7.1	0.0	7.4	0.0	14.3	7.1	10.7	0.0	14.8	3.6	7.1	7.4
Water	0.0	0.0	0.0	0.0	0.0	0.0	7.1	14.8	0.0	0.0	0.0	0.0

Bottom of Plant Canopy Percent Cover

Functional Group	Flux 3: 1995	Flux 3: 2021	Flux 4: 1995	Flux 4: 2021	Flux 6: 1995	Flux 6: 2021	Flux 7: 1995	Flux 7: 2021	Flux 8: 1995	Flux 8: 2021	Flux 10: 1995	Flux 10: 2021
Bryophyte	53.6	32.1	48.1	21.4	28.6	39.3	57.1	33.3	51.9	35.7	75.0	33.3
Deciduous	0.0	10.7	0.0	14.3	7.1	7.1	10.7	0.0	0.0	3.6	7.1	14.8
Evergreen	21.4	21.4	3.7	28.6	32.1	10.7	0.0	3.7	18.5	21.4	0.0	3.7
Forb	0.0	0.0	0.0	0.0	0.0	0.0	0.0	0.0	0.0	0.0	3.6	3.7
Graminoid	3.6	10.7	18.5	17.9	7.1	28.6	7.1	44.4	3.7	25.0	7.1	40.7
Lichen	3.6	0.0	7.4	10.7	7.1	3.6	0.0	0.0	3.7	7.1	0.0	0.0
Litter	17.9	25.0	22.2	7.1	14.3	10.7	17.9	7.4	22.2	7.1	7.1	3.7
Water	0.0	0.0	0.0	0.0	3.6	0.0	7.1	14.8	0.0	0.0	0.0	0.0

Table A1: Percent cover of functional groups in top and bottom of plant canopy, summed by plot in 1995 and 2021.

DATA AVAILABILITY STATEMENT

Flux plot field data was made available courtesy of Donald A. (Skip) Walker (personal communication, August 2021). Flux plot stereo triplets were rescanned at the resolution used for this study by Quantum Spatial (personal communication, February 2020).

Photogrammetry analysis was performed in Agisoft Metashape Professional (2016), and point cloud classification was done in R using the lidR package (Roussel, J.R & Auty, D. 2022). Sitemap was made using ArcGIS Pro (2021) and CHM maps were made in R.

REFERENCES

- Agisoft Metashape Professional (2016). (Version 1.8.1) [Software]. St. Petersburg Russia. Retrieved from <http://www.agisoft.com/downloads/installer/>
- Agisoft Metashape: User manuals. (2022). Agisoft.com. Retrieved March 10, 2022, from <https://www.agisoft.com/downloads/user-manuals/>
- ArcGIS Pro (2021). (Version 2.9.1) [Software]. Redlands, CA: Environmental Systems Research Institute.
- Alonzo M., Dial R.J., Schulz, B.K., Andersen, H.E., Lewis-Clark, E., Cook, B.D., & Morton D.C. (2000). Mapping tall shrub biomass in Alaska at landscape scale using structure-from-motion photogrammetry and lidar. *Remote Sensing of Environment*, 245, 111841. <https://doi.org/10.1016/j.rse.2020.111841>
- Auerbach, N.A., Walker, D.A. & Bockheim, J. (1996). Landcover of the Kuparuk River Basin, Alaska (map scale 1:500,000), University of Colorado, Boulder: Joint Facility for Regional Ecosystem Analysis.
- Berner, L.T., Massey, R., Jantz, P., Forbes, B.B., Macias-Fauria, M., Myers-Smith, I.H., et al. (2020). Summer warming explains widespread but not uniform greening in the Arctic tundra biome. *Nature Communications*, 11, 4621-4633. <https://doi:10.1038/s41467-020-18479-5>
- Bhatt, U.S., Walker, D.A., Raynolds, M.K., Bieniek, P.A., Epstein, H.E., Comisco, J.C., et al. (2013). Recent declines in warming and vegetation greening trends over Pan-Arctic Tundra. *Remote Sensing*, 5(9), 4229-4254 <https://doi.org/10.3390/rs5094229>
- Bjorkman, A.D., Myers-Smith, I.H., Elmendorf, S.C., Normand, S., Ruger, N., Beck, et al. (2018). Plant functional trait change across a warming tundra biome. *Nature*. 562, 57–62. <https://doi:10.1038/s41586-018-0563-7>
- Božek P., Janus J., & Mitka B. (2019). Analysis of Changes in Forest Structure using Point Clouds from Historical Aerial Photographs. *Remote Sensing*. 11(19), 2259. <https://doi:10.3390/rs11192259>
- Buckner, D.L. (1985). Point-intercept sampling in revegetation studies: maximizing objectivity and repeatability. *American Society for Surface Mining and Reclamation*, 110–114.
- Cao, L., Coops, N.C., Sun, Y., Ruan, H., Wang, G., Dai, J., She, G. (2019). Estimating canopy structure and biomass in bamboo forests using airborne LiDAR data. *ISPRS Journal of Photogrammetry and Remote Sensing*, 148, 114–129. <https://doi.org/10.1016/j.isprsjprs.2018.12.006>
- Carrivick J.L., Smith M.W., & Quincey D.J. (2016). *Structure from Motion in the Geosciences*. Hoboken, NJ: John Wiley & Sons.

- CAVM Team. (2003). Circumpolar Arctic Vegetation Map. (1:7,500,000 scale), *Conservation of Arctic Flora and Fauna (CAFF) Map No. 1*. U.S. Fish and Wildlife Service, Anchorage, Alaska. ISBN: 0-9767525-0-6, ISBN-13: 978-0-9767525-0-9
- Chapin, F. S., III. (2003). Effects of plant traits on ecosystem and regional processes: a conceptual framework for predicting the consequences of global change. *Annals of Botany*, 91(4), 455–463. <https://doi.org/10.1093/aob/mcg041>
- Chapin, F. S., Shaver, G. R., Giblin, A. E., Nadelhoffer, K. J., & Laundre, J. A. (1995). Responses of Arctic Tundra to Experimental and Observed Changes in Climate. *Ecology*, 76(3), 694–711. <https://doi.org/10.2307/1939337>
- Clement C. & Fraser R.H. (2017) Shrub monitoring in Canada’s Arctic using multi-scale measurements from field plots, unmanned aerial vehicles and satellite remote sensing (No. POLAR project PKC-NST-1617-004) (Polar Knowledge Canada)
- Cunliffe, A. M., Assmann, J., N Daskalova, G., Kerby, J. T., & Myers-Smith, I. H. (2020). Aboveground biomass corresponds strongly with drone-derived canopy height but weakly with greenness (NDVI) in a shrub tundra landscape. *Environmental Research Letters*, 15(12). <https://doi.org/10.1088/1748-9326/aba470>
- Cunliffe A. M, Brazier R. E. & Anderson K., (2016). Ultra-fine grain landscape-scale quantification of dryland vegetation structure with drone-acquired structure-from-motion photogrammetry, *Remote Sensing of Environment*. 183, 129–43. <https://doi.org/10.1016/j.rse.2016.05.019>
- Elmendorf, S.C., Henry, G.H.R, Hollister, R.D., Björk, R.G., Boulanger-Lapointe, N., Cooper, E.J., et al. (2012). Plot-scale evidence of tundra vegetation change and links to recent summer warming. *Nature Climate Change*. 2, 453–457. <https://doi.org/10.1038/nclimate1465>
- Epstein H.E., Reynolds M.K., Walker D.A., Bhatt, U.S., Tucker, C.J., & Pinzon, J.E. (2012). Dynamics of aboveground phytomass of the circumpolar Arctic tundra during the past three decades. *Environmental Research Letters*, 7, 015506-015518. <https://doi:10.1088/1748-9326/7/1/015506>
- Fraser R H, Olthof I., Lantz T.C., & Schmitt C. (2016). UAV photogrammetry for mapping vegetation in the low-Arctic. *Arctic Science*, 2(3), 79–102. <https://doi.org/10.1139/as-2016-0008>
- Frost G.V., Bhatt U.S., Epstein H.E., Walker, D.A., Reynolds, M.K., Berner, L.T., Bjerke, J.W., et al. (2019). Tundra Greenness in Arctic Report Card. Richter-Menge J, Druckenmiller M.L., and Jeffries M. Eds., <http://www.arctic.noaa.gov/Report-Card>
- Frost, G.V. & Epstein, H.E. (2013). Tall shrub and tree expansion in Siberia tundra ecotones since the 1960s. *Global Change Biology*, 20(4), 1264-1277. <https://doi.org/10.1111/gcb.12406>

- Greaves, H. E., Eitel, J. U. H., Vierling, L. A., Boelman, N. T., Griffin, K. L., Magney, T. S., & Prager, C. M. (2019). 20Cm Resolution Mapping of Tundra Vegetation Communities Provides an Ecological Baseline for Important Research Areas in a Changing Arctic Environment. *Environmental Research Communications*, 1(10). <https://doi.org/10.1088/2515-7620/ab4a85>
- Greaves, H. E., Vierling, L. A., Eitel, J. U. H., Boelman, N. T., Magney, T. S., Prager, C. M., & Griffin, K. L. (2015). Estimating aboveground biomass and leaf area of low-stature Arctic shrubs with terrestrial LiDAR. *Remote Sensing of Environment*, 164, 26–35. <https://doi.org/10.1016/j.rse.2015.02.023>
- Guay, K.C., Beck, P.S.A., Berner, L.T., Goetz, S.J., Baccini, A., & Buermann, W. (2014). Vegetation productivity patterns at high northern latitudes: a multi-sensor satellite data assessment. *Global Change Biology*, 20(10), 3147–3158 <https://doi.org/10.1111/gcb.12647>
- Helpdesk portal. (n.d.). Helpdesk Portal. Retrieved October 8, 2022, from <https://agisoft.freshdesk.com/support/solutions/articles/31000160729-parameters-for-ground-point-classification>
- Hudak, A.T. & Wessman, C.A. (1998). Textural Analysis of Historical Aerial Photography to Characterize Woody Plant Encroachment in South African Savanna. *Remote Sensing of Environment*, 66(3), 317-330. [https://doi.org/10.1016/s0034-4257\(98\)00078-9](https://doi.org/10.1016/s0034-4257(98)00078-9)
- AR5 Climate Change 2014: Impacts, Adaptation, and Vulnerability. (2014). Ipcc.Ch. Retrieved October 8, 2021, from <https://www.ipcc.ch/report/ar5/wg2/>
- Jorgenson, J. C., Reynolds, M. K., Reynolds, J. H., & Benson, A.-M. (2015). Twenty-five year record of changes in plant cover on tundra of northeastern Alaska. *Arctic, Antarctic, and Alpine Research*, 47(4), 785–806. <https://doi.org/10.1657/aaar0014-097>
- Kane, D. & Reeburgh, William. (1998). Introduction to special section: Land-Air-Ice Interactions (LAI) Flux Study. *Journal of Geophysical Research*, 1032. 28913-28916. <https://doi:10.1029/1998JD200017>
- Lisein, J., Pierrot-Deseilligny, M., Bonnet, S., Lejeune, P., (2013). A photogrammetric workflow for the creation of a forest canopy height model from small unmanned aerial system imagery. *Forests*, 4 (4), 922–944. <https://doi.org/10.3390/f4040922>
- Lillesand, T. M., Kiefer, R. W., & Chipman, J. W. (2008). *Remote Sensing and Image Interpretation*. Hoboken, NJ: John Wiley & Sons.
- Little, J.D., Sandall, H., Walegur, M.T., & Nelson, F.E. (2003). Application of Differential Global Positioning Systems to Monitor Frost Heave and Thaw Settlement in Tundra Environments. *Permafrost and Periglacial Processes*, 14(4), 349-357. <https://doi.org/10.1002/ppp.466>

- Liu, Q., Fu, L., Chen, Q., Wang, G., Luo, P., Sharma, R. P., He, P., Li, M., Wang, M., & Duan, G. (2020). Analysis of the spatial differences in canopy height models from UAV LiDAR and photogrammetry. *Remote Sensing*, 12(18), 1–22. <https://doi.org/10.3390/rs12182884>
- Lucas, R. M., Ellison, J. C., Mitchell, A., Donnelly, B., Finlayson, M., & Milne, A. K. (2002). *Wetlands Ecology and Management*, 10(2), 159–173. <https://doi.org/10.1023/a:1016547214434>
- Morgan, J.L., Gergel, S. E., & Coops, N. C. (2010). Aerial Photography: A Rapidly Evolving Tool for Ecological Management, *BioScience*, 60(1), 47-59. <https://doi.org/10.1525/bio.2010.60.1.9>
- Myers-Smith, I. H., Forbes, B. C., Wilmking, M., Hallinger, M., Lantz, T., Blok, D., et al. (2011). Shrub expansion in tundra ecosystems: dynamics, impacts and research priorities. *Environmental Research Letters*, 6(4), 045509. <https://doi.org/10.1088/1748-9326/6/4/045509>
- Myers-Smith, I. H., Grabowski, M. M., Thomas, H. J. D., Angers-Blondin, S., Daskalova, G. N., Bjorkman, et al. (2019). Eighteen years of ecological monitoring reveals multiple lines of evidence for tundra vegetation change. *Ecological Monographs*, 89(2), e01351. <https://doi.org/10.1002/ecm.1351>
- Myers-Smith, I. H., Kerby, J. T., Phoenix, G. K., Bjerke, J. W., Epstein, H. E., Assmann, J., et al. (2020). Complexity revealed in the greening of the Arctic. *Nature Climate Change*, 10(2), 106–117. <https://doi.org/10.1038/s41558-019-0688-1>
- Navarro, A., Young, M., Allan, B., Carnell, P., Macreadie, P., & Ierodiaconou, D. (2020). The application of Unmanned Aerial Vehicles (UAVs) to estimate above-ground biomass of mangrove ecosystems. *Remote Sensing of Environment*, 242, 111747. <https://doi.org/10.1016/j.rse.2020.111747>
- Pattison, R. R., Jorgenson, J. C., Reynolds, M. K., & Welker, J. M. (2015). Trends in NDVI and tundra community composition in the arctic of NE Alaska between 1984 and 2009. *Ecosystems*, 18(4), 707–719. <https://doi.org/10.1007/s10021-015-9858-9>
- Pinzon, J., & Tucker, C. (2014). A non-stationary 1981–2012 AVHRR NDVI3g time series. *Remote Sensing*, 6(8), 6929–6960. <https://doi.org/10.3390/rs6086929>
- Polar Research Board, Board on Life Sciences, Division on Earth and Life Studies, & National Academies of Sciences, Engineering, and Medicine. (2019). *Understanding northern latitude vegetation greening and browning: Proceedings of a workshop* (A. Melvin, Ed.). National Academies Press.

- Poley, L. G., & McDermid, G. J., (2020). A systematic review of the factors influencing the estimation of vegetation aboveground biomass using unmanned aerial systems. *Remote Sensing*, 12(7), 1052–1075. <https://doi.org/10.3390/rs12071052>
- R Core Team (2022). R: A language and environment for statistical computing. R Foundation for Statistical Computing, Vienna, Austria. [Software] <https://www.R-project.org/>
- Raynolds, M. K., & Walker, D. A. (2016). Increased wetness confounds Landsat-derived NDVI trends in the central Alaska North Slope region, 1985–2011. *Environmental Research Letters*, 11(8), 085004. <https://doi.org/10.1088/1748-9326/11/8/085004>
- Raynolds, M. K., Walker, D. A., Epstein, H. E., Pinzon, J. E., & Tucker, C. J. (2012). A new estimate of tundra-biome phytomass from trans-Arctic field data and AVHRR NDVI. *Remote Sensing Letters*, 3(5), 403–411. <https://doi.org/10.1080/01431161.2011.609188>
- Raynolds, M. K., Walker, D. A., Verbyla, D., & Munger, C. A. (2013). Patterns of change within a tundra landscape: 22-year Landsat NDVI trends in an area of the northern foothills of the Brooks range, Alaska. *Arctic, Antarctic, and Alpine Research*, 45(2), 249–260. <https://doi.org/10.1657/1938-4246-45.2.249>
- Rocha, A. V., & Wright, K. S. (2019). *ABOVE: MODIS- and CCAN-derived NDVI and trends, North Slope of Alaska, 2000-2015*. ORNL Distributed Active Archive Center. <https://doi.org/10.3334/ORNLDAAC/1666>
- Roussel, J.R., Auty, D., Coops, N. C., Tompalski, P., Goodbody, T. R. H., Sánchez, Meador, A., et al. (2020). lidR: An R package for analysis of Airborne Laser Scanning (ALS) data. *Remote Sensing of Environment*, 251(112061), 112061. <https://doi.org/10.1016/j.rse.2020.112061>
- Roussel, J.R., and Auty, D. (2022). Airborne LiDAR Data Manipulation and Visualization for Forestry Applications. (Version 4.0.0) [Software]. <https://cran.r-project.org/package=lidR>
- Schurr, T. (2019). Permafrost and the Global Carbon Cycle in Arctic Report Card, Richter-Menge J, Druckenmiller M.L., and Jeffries M. Eds. <http://www.arctic.noaa.gov/Report-Card>
- Shiklomanov, N.I., Streletskiy, D.A., Little, J.D., & Nelson, F.E., Isotropic thaw subsidence in undisturbed permafrost landscapes. *Geophysical Research Letters*, 40(24), 6356–6361. <https://doi.org/10.1002/2013GL058295>
- Sturm, M., Racine, C., & Tape, K. (2001). Climate change. Increasing shrub abundance in the Arctic. *Nature*, 411(6837), 546–547. <https://doi.org/10.1038/35079180>

- Tape, K., Sturm, M., & Racine, C. (2006). The evidence for shrub expansion in Northern Alaska and the Pan-Arctic: Shrub expansion in Northern Alaska and Par-Arctic. *Global Change Biology*, 12(4), 686–702. <https://doi.org/10.1111/j.1365-2486.2006.01128.x>
- Tremblay B, Lévesque E., and Boudreau S. (2012) Recent expansion of erect shrubs in the Low Arctic: evidence from Eastern Nunavik, *Environmental Research Letters*, 7, 035501, <https://doi:10.1088/1748-9326/7/3/035501>
- Tucker, C. J. (1979). Red and photographic infrared linear combinations for monitoring vegetation. *Remote Sensing of Environment*, 8(2), 127–150. [https://doi.org/10.1016/0034-4257\(79\)90013-0](https://doi.org/10.1016/0034-4257(79)90013-0)
- VanValkenburgh, P., Cushman, K. C., Butters, L. J. C., Vega, C. R., Roberts, C. B., Kepler, C., & Kellner, J. (2020). Lasers Without Lost Cities: Using Drone Lidar to Capture Architectural Complexity at Kuelap, Amazonas, Peru. *Journal of Field Archaeology*, 45(1), 575-588. <https://doi.org/10.1080/00934690.2020.1713287>
- Vepakomma, U., St-Onge, B., & Kneeshaw, D. (2008). Spatially explicit characterization of boreal forest gap dynamics using multi-temporal lidar data. *Remote Sensing of Environment*, 112(5), 2326–2340. <https://doi.org/10.1016/j.rse.2007.10.001>
- Walker, D.A & Bockheim, J. (1995). Summary of Field Activities email. North Slope ARCSS/LAII Flux Study
- Warhafting, C. (1965). Physiographic Divisions of Alaska. USGS Publications Warehouse, Professional Paper 462. <https://doi.org/10.3133/pp482>
- Walker, D.A. & Breen, AL., (2017). Pre-ABOVE: Arctic Vegetation Plots, ARCSS/LAII Flux Sites, North Slope, AK, 1995-1996. ORNL DAAC, Oak Ridge, Tennessee, USA. <https://doi.org/10.3334.ORNLDAAC/1535>
- Walker, M.D., Wahren, C., Hollister, R., Henry, G., Lorraine, El, Ahlquist, J., et al. (2006). Plant community responses to experimental warming across the tundra biome. *Proceedings of the National Academy of Sciences, USA*. 103(5),1342–1346. <https://doi.org/10.1073/pnas.050319810>
- Wookey P.A., Aerts, R., Bardgett, R.D., Baptist, F., Brathen, K.A., Cornelissen, J.H.C., et al., (2009). Ecosystem feedbacks and cascade processes: understanding their role in the responses of arctic and alpine ecosystems to environmental change, *Global Change Biology*, 15(5). 1153–72, <https://doi.org/10.1111/j.1365-2486.2008.01801.x>
- Xiao-Ying J., Hui-Jun J., Iwahana, G., Marchenko, S.S., Luo, D.L., Li, X.Y., & Liang, S.H. (2021). Impacts of climate-induced permafrost degradation on vegetation: A review. *Advances in Climate Change Research*, 12(1) 29-47 <https://doi.org/10.1016/j.accre.2020.07.002>

- Zhang, Q., Hu, M., Zhou, Y., Wan, B., Jiang, L., Zhang, Q., & Wang, D. (2022). Effects of UAV-LiDAR and Photogrammetric Point Density on Tea Plucking Area Identification. *Remote Sensing*, 14(6), 1505. <https://doi.org/10.3390/rs14061505>
- Zhang, T., Barry, R.G., Knowles, K., Ling, F., & Armstrong, R.L. (2003). Distribution of seasonally and perennially frozen ground in the Northern Hemisphere. In Phillips, M., Springman, S., Anderson, L.U., eds., *Proceedings of the Eighth International Conferences on Permafrost*, July 21-25, 2003, Zürich, Switzerland. Lisse, Balkema, 2, 1289-1294
- Zhang W., Qi J., Wan P., Wang H., Xie D., Wang X., Yan G. (2016). An Easy-to-Use Airborne LiDAR Data Filtering Method Based on Cloth Simulation. *Remote Sensing*, 8(6), 501. <https://doi.org/10.3390/rs8060501>